ImmunoTargets and Therapy Dovepress

Open Access Full Text Article ORIGINAL RESEARCH

Identification of CRTH2 as a New PPARγ-Target Gene in T Cells Suggested CRTH2 Dependent Conversion of T_h2 Cells as Therapeutic Concept in COVID-19 Infection

Antonia Becker[1], Karoline Röhrich[1], Amanda Leske[1], Ulrike Heinicke[1], Tilo Knape[2], Aimo Kannt[2,3], Verena Trümper[4], Kai Sohn[5], Annett Wilken-Schmitz[1], Holger Neb[1], Elisabeth H Adam[1], Volker Laux[2], Michael J Parnham[2], Valerie Onasch[4], Andreas Weigert[4], Kai Zacharowski[1,2], Andreas von Knethen[1]

[1]Goethe University Frankfurt, Department of Anaesthesiology, Intensive Care Medicine, and Pain Therapy, University Hospital Frankfurt, Frankfurt, 60590, Germany; [2]Fraunhofer Institute for Translational Medicine and Pharmacology ITMP, Frankfurt, 60596, Germany; [3]Institute of Clinical Pharmacology, Goethe University, Frankfurt, 60590, Germany; [4]Institute of Biochemistry I, Faculty of Medicine, Goethe-University Frankfurt, Frankfurt, 60590, Germany; [5]Innovation Field in-vitro Diagnostics, Fraunhofer Institute for Interfacial Engineering and Biotechnology IGB, Stuttgart, 70569, Germany

Correspondence: Andreas von Knethen, Email andreas.vonknethen@ukffm.de

Background: COVID-19 is a serious viral infection, which is often associated with a lethal outcome. Therefore, understanding mechanisms, which affect the immune response during SARS-CoV2 infection, are important.

Methods: To address this, we determined the number of T cells in peripheral blood derived from intensive care COVID-19 patients. Based on our previous studies, evaluating PPARγ-dependent T cell apoptosis in sepsis patients, we monitored PPARγ expression. We performed a next generation sequencing approach to identify putative PPARγ-target genes in Jurkat T cells and used a PPARγ transactivation assay in HEK293T cells. Finally, we translated these data to primary T cells derived from healthy donors.

Results: A significantly reduced count of total $CD3^+$ T lymphocytes and the $CD4^+$ and $CD8^+$ subpopulations was observed. Also, the numbers of anti-inflammatory, resolutive T_h2 cells and FoxP3-positive regulatory T cells (T_{reg}) were decreased. We observed an augmented PPARγ expression in $CD4^+$ T cells of intensive care COVID-19 patients. Adapted from a next generation sequencing approach in Jurkat T cells, we found the chemoattractant receptor-homologous molecule expressed on T helper type 2 cells (CRTH2) as one gene regulated by PPARγ in T cells. This T_h2 marker is a receptor for prostaglandin D and its metabolic degradation product 15-deoxy-Δ12,14-prostaglandin J_2 (15d-PGJ_2), an established endogenous PPARγ agonist. In line, we observed an increased PPARγ transactivation in response to 15d-PGJ_2 treatment in HEK293T cells overexpressing CRTH2. Translating these data to primary T cells, we found that T_h2 differentiation was associated with an increased expression of CRTH2. Interestingly, these $CRTH2^+$ T cells were prone to apoptosis.

Conclusion: These mechanistic data suggest an involvement of PPARγ in T_h2 differentiation and T cell depletion in COVID-19 patients.

Keywords: T_{reg}, PPARγ, T_h2, COVID-19, NGS, IL-4, CRTH2, FoxP3

Introduction

Serious infectious diseases leading to sepsis and/or multi organ failure (MOF; for a list of all used abbreviations see Supplementary Table 1) are often associated with a worse outcome.[1,2] Although recent data from severe COVID-19 patients show that they also could suffer from hyperactivation of the immune system associated with hyperinflammation,[3] one further mechanism contributing to the disease's severity is immune paralysis. This is mainly caused by the T cell depletion, blocking an adequate adaptive immune response.[4] In sepsis, T cell apoptosis seems to be the most important reason.[5–7] Thus, considering our data obtained in sepsis mouse models and following their translation to the human sepsis

Received: 9 February 2024
Accepted: 10 July 2024
Published: 2 November 2024

patient, we set up the hypothesis that in patients suffering from COVID-19, requiring intensive care, a similar mechanism is involved in a bad outcome.

Our previous findings in a mouse peritonitis model initiated by cecal ligation and puncture (CLP) to mimic peritonitis showed that expression and activation of the ligand-dependent transcription factor peroxisome proliferator-activated receptor γ (PPARγ) is responsible for T cell depletion, which is associated with immune paralysis.[8] Using T cell specific PPARγ knockout mice in a CLP polymicrobial sepsis model, T cell depletion, mainly mediated by T cell apoptosis, was prevented and mouse survival was improved.[7] Accordingly, treating wild type mice, suffering from CLP-induced peritonitis, with the irreversible PPARγ antagonist 2-chloro-5-nitro-N-phenylbenzamide (GW9662) provoked a similar protective effect.[8] Replacing the irreversible antagonist by a PPARγ-specific competitive antagonist,[9,10] more prone to be used therapeutically, proved a potential therapeutic concept.[11] Interestingly, isolation of cytotoxic T cells from CLP-treated mice, to follow ex–vivo cytotoxic T lymphocyte (CTL)-dependent cytotoxicity in an alloantigenic activation regime or using a classical splenocyte-driven activation protocol revealed that activation of PPARγ blocked CTL-dependent cytotoxicity toward alloantigenic target cells. This inhibition was absent in CTLs derived from T cell-specific PPARγ knockout mice.[12]

Translating these data to human T cells, we and others found that PPARγ is expressed in activated primary, blood derived T cells,[13,14] sensitizing these cells to PPARγ-dependent apoptosis.[13,15] In T cells derived from blood of sepsis patients, PPARγ was also expressed.[16] Plasma, obtained from these patients induced PPARγ-activation in a Jurkat PPRE-containing reporter cell line, suggesting the existence of an endogenous PPARγ activator in the blood,[16] such as 15-deoxy-Δ12,14-prostaglandin J_2 (15d-PGJ_2).[17,18] Finally, a link was shown between the level of PPARγ expression and the T cell number in sepsis patients.[19] In the same study, high PPARγ mRNA expression was correlated to a lower T cell count, which was associated with a worse outcome of the patients.[19] However, PPARγ expression was only determined on mRNA level.

Mechanistically, PPARγ-dependent T cell apoptosis has been described to be mediated by the induction of the phosphatase and tensin homolog (PTEN), counteracting protein kinase B activation[20] and by scavenging the transcription factor nuclear factor of activated T cells (NF-AT), consequently transrepressing for instance expression of the T cell pro-survival cytokine IL-2.[8,21] Possibly, also a functional shift of PPARγ from its DNA-binding requiring role to a non-DNA-linked effect might be involved.[22] However, only insufficient knowledge about T cell-specific target genes regulated following PPARγ expression and activation is at hand.

Based on these data, we focused our interest first on the determination of an mRNA profile of T cell-dependent expression of PPARγ target genes. Then, we analyzed whether T cells are also depleted in the blood of intensive care COVID-19 patients and whether PPARγ is expressed in COVID-19 patients´ T cells, sensitizing these cells towards cell death, consequently counteracting an adequate immune response.

Materials and Methods

Chemical Reagents

All chemicals and reagents were of the highest grade of purity. The PPARγ antagonist, GW9662 (#70785),[23] was acquired from Cayman Chemical Company (Ann Arbor, USA) and the PPARγ agonists, rosiglitazone (#R2408)[24] and the PGD_2 derivative 15-deoxy-Δ12,14-prostaglandin J_2 (15d-PGJ_2, #D8440)[18,25] were bought from Sigma-Aldrich (Merck KGaA, Darmstadt, Germany).

Cell Culture

The human T cell line Jurkat[26] (DSMZ, ACC282) was cultured in Roswell Park Memorial Institute (RPMI) 1640 and the human embryonic kidney cell line HEK293T[27] (ATCC, CRL-3216) in Dulbecco`s Modified Eagle`s Medium (DMEM) high glucose in a humidified 5% carbon dioxide (CO_2) atmosphere at 37°C. Both media were supplemented with 10% (v/v) heat-inactivated fetal calf serum (FCS), 100 units/mL penicillin and 100 µg/mL streptomycin. The medium was changed three times a week and cells passaged before reaching confluence.

Generation of Jurkat T Cells with a Tet-Inducible Expression of PPARγ

To generate Jurkat T cells with a Tet-inducible expression of PPARγ, we cloned human PPARγ1 (accession-no. NM_138712) into the lentiviral vector pLVX-TRE3G-mCherry (#631360, TaKaRa) according to the distributor's instructions. Briefly, the vector, containing an IRES-site to allow expression of mCherry and PPARγ1 as separate proteins, was cut with MluI/EcoRI. Human PPARγ1 was amplified using CloneAmp HiFi PCR Premix (#639298, TaKaRa), the forward primer 5´-GCC CCC GGG ACG CGT ATG ACC ATG GTT GAC ACA GAG ATG-3´, the reverse primer 5´- CTA CCC GGT AGA ATT CGT ACA AGT CCT TGT AGA TCT CCT G-3´ and a human PPARγ1 containing vector as template.[22] The primer pair (biomers.net GmbH, Ulm, Germany) was selected to allow In-Fusion cloning (#639650, TaKaRa) into the MluI/EcoRI site of the pLVX-TRE3G-mCherry vector. The correct sequence of the cloned vector was verified by restriction digestion with BamHI/XhoI and sequencing. The vector was transduced into the Jurkat Tet-On® 3G cell line (#631181, TaKaRa). Importantly, these cells must be cultured in RPMI1640 with Tet system approved FCS (#631106, TaKaRa). Following treatment of the transduced cells with 2 µg/mL doxycycline to induce target gene expression, first mCherry-positive cells were enriched by FACS-sorting using the BD FACSAria™ III cell sorter (BD Biosciences). Secondly, we performed a Western blot from lysates of these cells to verify expression of PPARγ1 as well (Supplementary Figure 1). These cells were used for the sequencing approach to identify PPARγ target genes in Jurkat T cells. Thus, doxycycline-treated cells were stimulated with the PPARγ agonist rosiglitazone [1 µM] alone, or in combination with the irreversible PPARγ antagonist GW9662 [10 µM] for 24 h. Afterwards cells were harvested for RNA isolation (Supplementary Figure 2).

RNA Extraction

RNA isolation was performed using the QIAcube (Qiagen) and the RNeasy Plus Mini Kit according to the manufacturer's protocol. Therefore, cell pellets were resuspended in 350 µL RLT Plus Buffer and vortexed for two minutes. The whole sample was than used for loading as a start material into the QiaCube. Nucleic acids were eluted in 30 µL molecular grade water. The quantity and quality of the isolated RNA was determined with a Qubit Fluorometer 3.0 (Life Technologies) and a Fragment Analyzer (Agilent), respectively.

Preparation of NGS Libraries and Sequencing

For transcriptome analysis 100 ng total RNA of each sample were automated prepared by using the TruSeq mRNA v2 Kit from (Illumina) on a Biomek FXP (Beckman Coulter). Libraries were quantified with the Qubit dsDNA HS Assay Kit (Life Technologies) and quality was assessed by the High Sensitivity NGS Kit on a Fragment Analyzer 5200 (Agilent). Sequencing of libraries was performed on HiSeq2500 (Illumina), resulting in 30 million 50-bp single-end reads per sample. After de-multiplexing with the Illumina's software bcl2fastq-1.8.4 with default settings for adapter trimming (at least 90% of bases should match) and no mismatches allowed in sequencing barcode, all reads undergo quality-based trimming to remove potential contaminants, low quality reads and sequencing adapters with the help of BBDuk from the BBMap package version 34.41 (https://sourceforge.net/projects/bbmap/). To pass the quality filter, read quality needed to be higher than a Phred score of 20 and achieve a minimal length of 50 bp after quality-based and adapter trimming. Additionally, every sample was quality-controlled before and after trimming with the FastQC (http://www.bioinformatics.babraham.ac.uk/projects/fastqc/). FastQC evaluates per base sequence quality, average base composition, GC content, sequence length distribution and adapter contaminations after trimming.

Bioinformatics Quantification and Differential Expression Profiling

Reads were mapped against the human reference genome (GRCh38) using NextGenMap 0.5.5 with default settings. Quantification of genes in RPKM (= reads per kilobase of exon model per million) mapped reads according to Mortazavi et al[28] was carried out exclusively with uniquely mapped reads using Genecode annotation v21 using the python script "rpkmforgenes.py" from the RSeQC package.[29] Additional QC step involves cross-comparison between replicates, which includes calculation of correlation matrices and pair-wise scatterplots comparison for each replicate. Differential expression analysis performed in R Bioconductor using EdgeR[30,31] and DESeq2 packages.[32] Cut-off-points were set as log2 fold change of at least +1 or −1 with p = 0.05 or less.

Blood Samples

We analysed leukocyte subsets from peripheral blood samples in citrate tubes derived from COVID-patients daily during their ICU stay. Patients were included when being positive for COVID-19 and showing already a serious respiratory and/or systemic symptomatology (n = 24). The study was performed in accordance with the Declaration of Helsinki. Approval from the local ethics committee of University Department of Medicine, Goethe-University Frankfurt, was obtained before the study was conducted (reference #20-643, #20-982) and a waiver regarding the requirement of written informed consent from COVID-19 patients was authorized by the local ethics committee of the University Department of Medicine, Goethe University Frankfurt, due to the intensive care-dependent sedation, and ventilation, and the patients` unconsciousness, which made it disproportionate to obtain a patient´s approval in advance during COVID-19 crisis. All participants of the control group provided written informed consent. The experimental setup of this part of our study is shown in Figure 1. The corresponding gating strategy is provided in Supplementary Figure 3. Following erythrocyte lysis, leukocytes were stained for CD3-APC-Vio-770 (#130-113-126), CD4-VioGreen (#130-113-221), CD8-PerCP (#130-113-160), FoxP3-APC (#130-125-580), and CRTH2-PE (#130-113-600) with antibodies bought from Miltenyi-Biotec (Bergisch-Gladbach, Germany). Intracellular staining of FoxP3 was done using the FoxP3 staining buffer set (#130-093-142, Miltenyi Biotec, Bergisch Gladbach, Germany) according to the manufacturer´s protocol. Cell counts were calculated using CountBright Absolute Counting Beads (#C36950, Invitrogen, Thermo Fisher, Dreieich, Germany).

Intracellular staining for PPARγ expression was established using the FoxP3 staining buffer set as outlined above and a polyclonal rabbit anti-PPARγ antibody labelled with Alexa Fluor750 (#BSS-BS-4590R-A750, Biozol Diagnostica) and the identical clone unconjugated (#BSS-BS-4590R). As a PPARγ unspecific antibody an α-FoxP3 antibody was used (#130-125-580, Miltenyi Biotec) (Supplementary Figure 4).

Analysis of blood samples was performed with a BD FACS Canto II flow cytometer (BD Biosciences) and FlowJo software (Version 10.8.1, Ashland, U.S.A).

Enrichment of Human Primary CD4+ Cells

To purify $CD4^+$ T cells from peripheral blood of healthy volunteers, citrate blood was diluted 1:2 with Dulbecco's phosphate-buffered saline without $Ca^{2+/}Mg^{2+}$ (DPBS, #D8537, Sigma-Aldrich, Merck KGaA, Darmstadt, Germany).

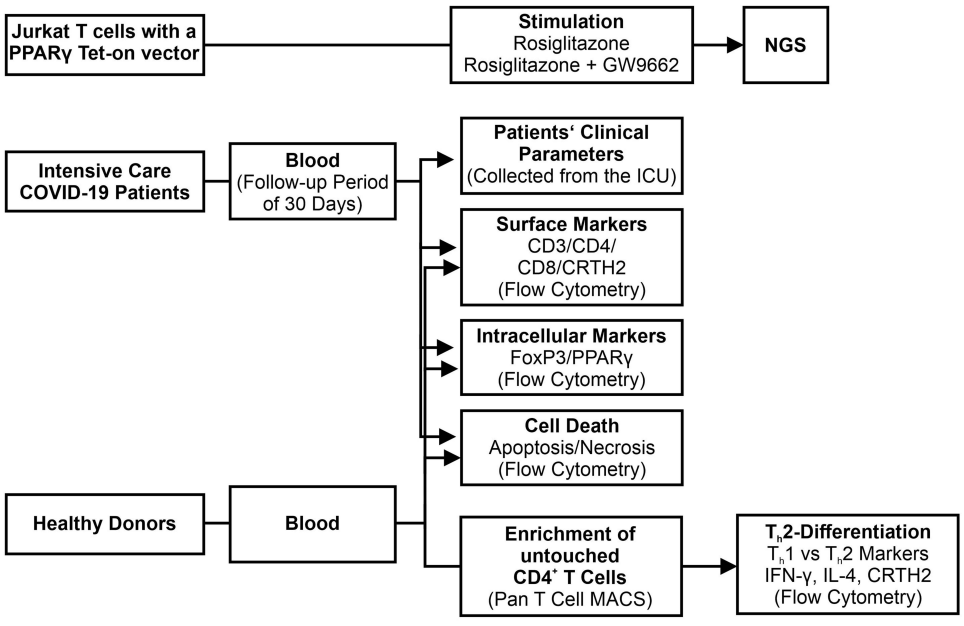

Figure 1 Study design.

Abbreviations: CD, cluster of differentiation; COVID-19, coronavirus disease 2019; CRTH2, chemokine receptor homologue expressed on T_h2 cells; FoxP3, forkhead box protein 3; GW9662, 2-chloro-5-nitro-N-phenylbenzamide; ICU, intensive care unit; IFN-γ, interferon-γ; IL-4, interleukin 4; MACS, magnetic cell sorting; NGS, next generation sequencing; PPARγ, peroxisome proliferator activated receptor γ; Tet, tetracycline; T_h1, T helper cells type 1; T_h2, T helper cells type 2.

This mixture was loaded onto a 50 mL Leucosep™ tube (#227290, Greiner Bio-One GmbH, Frickenhausen, Germany) which already contained 15 mL Pancoll human (#P04-60500, PAN™ Biotech) separation medium. Tubes were centrifuged for 20 min at 800 x g at room temperature (RT). Centrifuge brakes have been disabled to maintain phase separation following centrifugation. The phase containing peripheral blood mononuclear cells (PBMCs) was washed three times with 10 mL DPBS for 5 min at 300 × g at 4°C. From these PBMCs, $CD4^+$ T cells were enriched using magnetic cell sorting (MACS) with the $CD4^+$ T cell isolation kit, human (#130-096-533, Miltenyi-Biotec). To achieve this, 1×10^7 cells of the PBMCs were diluted in 40 µL autoMACS® rinsing solution (#130-091-222, Miltenyi-Biotec), containing 5% MACS® bovine serum albumin (BSA) stock solution (#130-091-376, Miltenyi-Biotec). After adding 10 µL of the $CD4^+$ T cell biotin antibody cocktail, cells were incubated on ice for 5 min. Then, 30 µL autoMACS rinsing solution was added together with 20 µL $CD4^+$ T cell MicroBead cocktail. After 10 min incubation on ice, the volume of the cell suspension was increased to 500 µL with autoMACS rinsing buffer. A LS separation column (#130-042-401, Miltenyi-Biotec) was positioned on a MidiMACS® separator (#130-042-302, Miltenyi-Biotec) and prewashed with 3 mL supplemented autoMACS rinsing buffer. Then, the cell suspension was loaded on the prepared column. Negative, ie $CD4^-$, cells were eluted twice with 3 mL autoMACS rinsing buffer, before the column was removed from the MidiMACS separator and positive $CD4^+$ cells were eluted twice with 3 mL autoMACS rinsing solution. Enrichment was roughly 96% $CD4^+$ T cells (Supplementary Figure 5).

T_h2-Differentiation

Following isolation of $CD4^+$ T cells, these cells were differentiated to T_h2 cells with CellXVIVO™ Human T_h2 Differentiation Kit (#CDK002, R&D Systems, Bio-Techne GmbH, Wiesbaden, Germany). The day before, the 24-well plate was coated with mouse-anti-human CD3, diluted to 1-fold, per well. The plates were incubated over night at 4°C and before using, washed twice with 1-fold washing buffer. 1×10^5 and 2×10^5 enriched $CD4^+$ cells were resuspended in 1 mL of T_h2-differentiation medium containing X–Vivo15™ cell medium, 100 U/mL penicillin, 100 µg/mL streptomycin and human T_h2 reagents included in the kit. Afterwards, cells were seeded into an already coated well. To achieve differentiation to a T_h2 phenotype, cells were incubated for 13 days, with a medium change every two to four days, by replacing 900 µL old medium with 900 µL new T_h2 differentiation medium. If necessary, cells were splitted. At day 13, efficacy of differentiation was determined by FACS analysis. For this purpose, cells were directly stained for the intracellular T_h2 marker cytokine IL-4 and the T_h1 indicator IFN-γ (Supplementary Figure 6A). Additionally, this intracellular staining was performed in cells which were washed once in X-Vivo 15™ cell medium (Lonza, Cologne, Germany) and resuspended in cell medium supplemented with antibiotics as described above, incubated for 6 h with a 1-fold cell activation cocktail (#5476, Tocris, Bristol, UK) containing phorbol myristate acetate (PMA) and ionomycin for cell activation, and monensin to block cytokine export (Supplementary Figure 6B). To allow an effective intracellular retention of IL-4, BD GolgiPlug™ (#555029, BD Biosciences), containing brefeldin A, was added in parallel.[33] Intracellular cytokines were stained using the FoxP3 staining buffer set (#130-093-142, Miltenyi-Biotec). To determine whether PPARγ is involved in T_h2 differentiation, we performed one set of experiments where we added 10 µM of the PPARγ antagonist GW9662 to the T_h2 differentiation as described above. After 13 days, the cells were stained for IL-4 and CRTH2.

Cell Death Determination

Following incubations, 2×10^5 cells were labeled with 5 µL annexin V-PE (#31490014, ImmunoTools, Friesoythe, Germany) and 10 µL 7-aminoactinomycin D (7-AAD, #130-111-568, Miltenyi-Biotec) in 100 µL binding buffer for 15 min on ice in the dark to differentiate between apoptotic and necrotic cell death. Afterwards, 150 µL binding buffer was added, and cell samples were analyzed immediately using a FACSCanto II flow cytometer and FlowJo software (Version 10.8.1, Ashland, U.S.A). Apoptosis was assessed when cells were annexin V-PE-positive. Accordingly, only 7-AAD-positive cells were considered as necrotic. PE vs R-phycoerythrin (PE)-Cy®5 fluorescences of a minimum of 10,000 cells were analysed. In some experiments annexin-V –FITC (#556420, Pharmingen, BD Biosciences, Heidelberg, Germany) was used instead of annexin V-PE. Accordingly, the extinction/emission wavelength filter setting was changed.

Peroxisome Proliferator Responsive Element (PPRE) Reporter Gene Assay

The p(A-Ox3)-TK-FL plasmid, containing three copies of the PPRE site derived from the human acyl coenzyme A oxidase (A-Ox) gene promoter cloned upstream of the thymidine kinase (TK) minimal promoter and the firefly luciferase (FL) gene, was transfected into the HEK293T cells using jetPEI (Polyplus, Illkirch, France), according to the manufacturer's instructions. Briefly, 10.000 HEK293T cells were seeded in 100 µL medium one day before transfection per well in a 96-well plate. Simultaneously, a PPARγ wt vector (pcDNA3-PPARγ wt) or a PPARγ d/n-encoding plasmid (pcDNA3-PPARγ AF2), containing two amino acid exchanges (Leu468Ala/Glu471Ala) and preventing ligand binding and concomitant activation of PPARγ,[34] were transfected as well. Finally, to estimate transfection efficiency a vector encoding renilla luciferase (RL) driven by a CMV promoter (pRL-CMV, #E2261, Promega, Walldorf, Germany) was also transfected. Cells were treated as indicated. After harvesting and lysing cells, extracts were assayed for renilla and firefly luciferase activity with the Dual-GloR Luciferase Assay System (#E2920, Promega, Walldorf, Germany).

Statistical Analysis

We used two-tailed statistical analysis to evaluate the data. Results are expressed as the mean or median ± SD. ANOVA, Mann–Whitney *U*-test, Kruskal–Wallis test, one sample *t* test, Dunn's multiple comparison test, and Student's *t*-test were used where appropriate. We considered P values ≤ 0.05 as statistically significant.

Results

mRNA Transcriptome Analysis of PPARγ Target Genes Expression in Jurkat T Cells

To address this question, we determined the PPARγ-dependent mRNA profile in Jurkat T cells. To acknowledge the possibility of a pro-apoptotic role of constitutive PPARγ expression, we used a vector system for a Tet-on inducible PPARγ expression. Following selection of positive clones, we used these for transcriptome profiling. First, we determined the mRNA profile of Jurkat T cells expressing PPARγ with activation by the specific agonist rosiglitazone (Supplementary Figure 2, upper part). Based on this treatment we obtained a panel of regulated genes shown in Table 1. To further validate a PPARγ-dependent gene induction mechanism, we treated the cells with a combination of the PPARγ agonist rosiglitazone and the irreversible PPARγ antagonist GW9662 (Supplementary Figure 2, lower part).[23,24] Following this treatment, RNA-seq revealed a panel of genes, which upon rosiglitazone treatment have been upregulated but in response to the simultaneous addition of GW9662 remained downregulated (Table 2). In summary, 55 genes were up- and 1 gene was down-regulated by rosiglitazone, whereas only 4 genes were up-, but 38 genes were downregulated after the parallel stimulation of the cells with rosiglitazone and GW9662 (Figure 2). Among others, PPARγ activation induced the prostaglandin D2 receptor 2 gene (PTGDR2, Table 1, line 4), and PPARγ antagonism kept PTGDR2 expression low (Table 2, next to last line), indicating a PPARγ-responsive expression in Jurkat T cells. Interestingly, this surface marker is also known as chemoattractant receptor-homologous molecule expressed on T helper type 2 cells (CRTH2). Thus, it can bind to PGD_2 and as well to its dehydration end product 15-deoxy-Δ12,14-prostaglandin J_2 (15d-PGJ_2),[17] which is an endogenous agonist of PPARγ.[25] Activation of CRTH2 has been shown to polarize T_h cells to the more anti-inflammatory, resolutive T_h2 phenotype.[35] With this new information on PPARγ-dependent alteration in T cell expression, we went on to determine the T cell number in intensive care COVID-19 patients.

Decreased T Cell Number in Peripheral Blood Derived from COVID-19 Patients Show a T_h2 Shift, Associated with PPARγ

To prove the assumption of a role of PPARγ in COVID-19-dependent T cell depletion and shifting the T cell phenotype from T_h1 to T_h2 cells, we determined the T cell subpopulations in peripheral blood drawn from COVID-19 patients during their ICU stay starting from day 1, requiring intensive care support, to day 30. Patients' demographics are presented in Table 3. We compared these T cell numbers to the T cell count of healthy volunteers, whose demographics are shown in Table 4. Moreover, referencing literature data of 600–3100 $CD3^+$ T cells/µL blood, the quantity of CD3 T^+ cells ab initio was significantly reduced in the blood derived from COVID-19 patients (Figure 3A). Focussing on the T cell subpopulations T helper (T_h) cells ($CD4^+$) and cytotoxic T cells (CTL, $CD8^+$), we found a significant reduction of both T cell types (Figure 3B and C) over the complete period of the ICU stay. However remarkably, on the last day in the

Table 1 Regulated Genes in Jurkat T Cells in Response to Rosiglitazone-Dependent Activation of PPARγ

HGNC symbol	Description	Ensembl ID	logFC	logCPM	Pvalue	FDR
AGXT	Alanine-glyoxylate aminotransferase	ENSG00000172482	9,83	1,35	8,18E-23	2,57E-19
ZP1	Zona pellucida glycoprotein 1 (sperm receptor)	ENSG00000149506	4,12	2,14	1,71E-15	2,09E-12
PTGDR2	Prostaglandin D2 receptor 2	ENSG00000183134	4,11	3,82	3,10E-46	3,41E-42
S100P	S100 calcium binding protein P	ENSG00000163993	3,93	2,71	1,84E-30	6,74E-27
CREB3L3	cAMP responsive element binding protein 3-like 3	ENSG00000060566	3,19	8,66	9,60E-87	2,11E-82
BTN1A1	Butyrophilin, subfamily 1, member A1	ENSG00000124557	3,17	1,96	2,70E-09	1,41E-06
CYP4F12	Cytochrome P450, family 4, subfamily F, polypeptide 12	ENSG00000186204	2,76	2,08	2,96E-10	1,75E-07
CNTFR	Ciliary neurotrophic factor receptor	ENSG00000122756	2,73	2,23	1,72E-11	1,40E-08
MARCO	Macrophage receptor with collagenous structure	ENSG00000019169	2,51	2,45	6,64E-12	5,84E-09
KIAA1683	KIAA1683	ENSG00000130518	2,47	1,57	3,03E-11	2,15E-08
FGR	FGR proto-oncogene, Src family tyrosine kinase	ENSG00000000938	2,33	2,05	4,58E-11	3,15E-08
H2AFY2	H2A histone family, member Y2	ENSG00000099284	2,03	2,59	9,11E-07	2,75E-04
LAMB2	Laminin, beta 2 (laminin S)	ENSG00000172037	1,97	2,76	7,07E-13	7,41E-10
GRM4	Glutamate receptor, metabotropic 4	ENSG00000124493	1,93	2,92	1,23E-12	1,18E-09
AHNAK	AHNAK nucleoprotein	ENSG00000124942	1,91	4,53	4,40E-17	6,06E-14
ARHGAP31	Rho GTPase activating protein 31	ENSG00000031081	1,90	4,58	1,48E-20	4,08E-17
CD9	CD9 molecule	ENSG00000010278	1,86	2,83	2,06E-08	8,55E-06
CD52	CD52 molecule	ENSG00000169442	1,86	5,97	6,34E-36	3,49E-32
SEC31B	SEC31 homolog B, COPII coating complex component	ENSG00000075826	1,86	5,80	7,70E-06	1,78E-03
ITGAL	Integrin, alpha L (antigen CD11A (p180), lymphocyte function-associated antigen 1; alpha polypeptide)	ENSG00000005844	1,84	8,44	2,56E-41	1,88E-37
CEACAM1	Carcinoembryonic antigen-related cell adhesion molecule 1 (biliary glycoprotein)	ENSG00000079385	1,74	2,98	1,61E-11	1,36E-08
FLRT1	Fibronectin leucine rich transmembrane protein 1	ENSG00000126500	1,66	1,68	5,22E-06	1,31E-03
MS4A7	Membrane-spanning 4-domains, subfamily A, member 7	ENSG00000166927	1,64	1,11	7,12E-05	1,18E-02
GOLGA7B	Golgin A7 family, member B	ENSG00000155265	1,63	1,33	2,98E-04	3,81E-02
KLF2	Kruppel-like factor 2	ENSG00000127528	1,61	4,56	2,96E-11	2,15E-08
LTB	Lymphotoxin beta (TNF superfamily, member 3)	ENSG00000227507	1,60	1,94	1,10E-06	3,23E-04
KIAA1522	KIAA1522	ENSG00000162522	1,57	6,02	1,31E-31	5,74E-28
TLR5	Toll-like receptor 5	ENSG00000187554	1,54	2,05	5,02E-05	8,84E-03
C15orf52	Chromosome 15 open reading frame 52	ENSG00000188549	1,49	1,09	6,86E-05	1,14E-02
TMEM91	Transmembrane protein 91	ENSG00000142046	1,46	1,31	2,34E-04	3,15E-02
GSDMB	Gasdermin B	ENSG00000073605	1,46	4,45	4,16E-04	4,94E-02

(*Continued*)

Table 1 (Continued).

HGNC symbol	Description	Ensembl ID	logFC	logCPM	Pvalue	FDR
SLC25A20	Solute carrier family 25 (carnitine/acylcarnitine translocase), member 20	ENSG00000178537	1,41	5,54	2,60E-18	4,40E-15
KRT2	Keratin 2, type II	ENSG00000172867	1,38	1,57	1,12E-04	1,75E-02
PHLDA1	Pleckstrin homology-like domain, family A, member 1	ENSG00000139289	1,36	2,56	1,22E-05	2,74E-03
SUSD4	Sushi domain containing 4	ENSG00000143502	1,34	4,70	2,35E-11	1,85E-08
CELSR1	Cadherin, EGF LAG seven-pass G-type receptor 1	ENSG00000075275	1,31	4,29	3,60E-08	1,37E-05
LAT2	Linker for activation of T cells family, member 2	ENSG00000086730	1,28	1,71	7,21E-05	1,18E-02
KBTBD8	Kelch repeat and BTB (POZ) domain containing 8	ENSG00000163376	1,25	3,66	2,51E-08	1,02E-05
SLC5A3	Solute carrier family 5 (sodium/myo-inositol cotransporter), member 3	ENSG00000198743	1,25	6,40	1,10E-06	3,23E-04
KCNK5	Potassium channel, two pore domain subfamily K, member 5	ENSG00000164626	1,25	6,12	3,78E-19	6,92E-16
IL7R	Interleukin 7 receptor	ENSG00000168685	1,21	4,43	1,52E-07	5,05E-05
TNFRSF1B	Tumor necrosis factor receptor superfamily, member 1B	ENSG00000028137	1,20	1,65	3,60E-04	4,40E-02
NKG7	Natural killer cell granule protein 7	ENSG00000105374	1,19	1,97	1,22E-04	1,90E-02
BCL6	B-cell CLL/lymphoma 6	ENSG00000113916	1,19	4,55	4,54E-08	1,69E-05
CACNA2D4	Calcium channel, voltage-dependent, alpha 2/delta subunit 4	ENSG00000151062	1,18	3,45	6,29E-07	1,95E-04
ATP2A1	ATPase, Ca++ transporting, cardiac muscle, fast twitch 1	ENSG00000196296	1,16	3,04	1,48E-05	3,25E-03
SH2D2A	SH2 domain containing 2A	ENSG00000027869	1,15	3,52	1,07E-07	3,61E-05
TMEM229B	Transmembrane protein 229B	ENSG00000198133	1,14	3,66	6,21E-06	1,50E-03
PPP2R3A	Protein phosphatase 2, regulatory subunit "B", alpha	ENSG00000073711	1,12	2,74	2,36E-04	3,16E-02
HAS3	Hyaluronan synthase 3	ENSG00000103044	1,07	2,34	2,74E-04	3,57E-02
CHCHD10	Coiled-coil-helix-coiled-coil-helix domain containing 10	ENSG00000250479	1,06	3,79	1,72E-04	2,53E-02
CCRL2	Chemokine (C-C motif) receptor-like 2	ENSG00000121797	1,05	2,95	1,87E-05	4,03E-03
ADM	Adrenomedullin	ENSG00000148926	1,04	3,11	3,04E-05	5,91E-03
BTNL9	Butyrophilin-like 9	ENSG00000165810	1,03	5,00	7,84E-06	1,80E-03
MME	Membrane metallo-endopeptidase	ENSG00000196549	1,03	3,05	3,41E-04	4,21E-02
GPR65	G protein-coupled receptor 65	ENSG00000140030	−1,06	1,82	4,22E-04	5,00E-02

Notes: Green cells: upregulated; orange cells: downregulated.

ICU, ie, day 30, the count of $CD8^+$ cells tended to recover, thus the reduction was no longer significant (Figure 3C, last column). Interestingly, the $CD4^+/CD8^+$ ratio remained almost completely unaltered during the complete 30 days stay compared to healthy donors (Figure 3D). Comparing non-ventilated, ventilated, and ECMO-receiving patients, the

Table 2 Regulated Genes in Jurkat T Cells in Response to the Parallel Incubation with the PPARγ Agonist Rosiglitazone and the Irreversible PPARγ Antagonist GW9662

HGNC Symbol	Description	Ensembl ID	logFC	logCPM	Pvalue	FDR
ZNF780B	Zinc finger protein 780B	ENSG00000128000	1,31	1,93	2,68E-04	3,56E-02
COL4A4	Collagen, type IV, alpha 4	ENSG00000081052	1,20	1,22	2,87E-04	3,69E-02
GPR65	G protein-coupled receptor 65	ENSG00000140030	1,12	1,93	6,89E-05	1,25E-02
CYP46A1	Cytochrome P450, family 46, subfamily A, polypeptide 1	ENSG00000036530	1,03	2,01	4,44E-05	8,88E-03
NR2F2	Nuclear receptor subfamily 2, group F, member 2	ENSG00000185551	−1,00	3,97	7,08E-06	1,97E-03
RNF182	Ring finger protein 182	ENSG00000180537	−1,02	1,43	4,21E-04	4,98E-02
SPSB1	splA/ryanodine receptor domain and SOCS box containing 1	ENSG00000171621	−1,03	5,16	3,19E-11	2,81E-08
LTB	Lymphotoxin beta (TNF superfamily, member 3)	ENSG00000227507	−1,09	2,13	2,24E-04	3,12E-02
CHCHD10	Coiled-coil-helix-coiled-coil-helix domain containing 10	ENSG00000250479	−1,10	3,84	2,66E-04	3,55E-02
HAS3	Hyaluronan synthase 3	ENSG00000103044	−1,11	2,39	6,00E-06	1,69E-03
SH2D2A	SH2 domain containing 2A	ENSG00000027869	−1,13	3,58	6,43E-08	2,95E-05
TMEM229B	Transmembrane protein 229B	ENSG00000198133	−1,17	3,71	4,55E-06	1,30E-03
GPC4	Glypican 4	ENSG00000076716	−1,21	3,72	9,31E-08	4,18E-05
CDC42EP4	CDC42 effector protein (Rho GTPase binding) 4	ENSG00000179604	−1,22	1,66	8,29E-05	1,45E-02
FAM167A	Family with sequence similarity 167, member A	ENSG00000154319	−1,28	2,70	2,41E-07	9,99E-05
TNFRSF1B	Tumor necrosis factor receptor superfamily, member 1B	ENSG00000028137	−1,29	1,67	5,67E-05	1,08E-02
LAMB2	Laminin, beta 2 (laminin S)	ENSG00000172037	−1,29	2,98	3,72E-06	1,09E-03
KLF2	Kruppel-like factor 2	ENSG00000127528	−1,31	4,70	3,18E-07	1,25E-04
KCNK5	Potassium channel, two pore domain subfamily K, member 5	ENSG00000164626	−1,32	6,16	3,16E-21	1,16E-17
PPP2R3A	Protein phosphatase 2, regulatory subunit "B", alpha	ENSG00000073711	−1,35	2,73	2,39E-05	5,66E-03
FGR	FGR proto-oncogene, Src family tyrosine kinase	ENSG00000000938	−1,36	2,30	1,36E-05	3,39E-03
SUSD4	Sushi domain containing 4	ENSG00000143502	−1,41	4,74	1,48E-11	1,36E-08
CEACAM1	Carcinoembryonic antigen-related cell adhesion molecule 1 (biliary glycoprotein)	ENSG00000079385	−1,44	3,11	4,87E-09	3,06E-06
CD9	CD9 molecule	ENSG00000010278	−1,44	2,98	1,22E-04	1,99E-02
KIAA1522	KIAA1522	ENSG00000162522	−1,48	6,11	5,76E-27	4,22E-23
GRM4	Glutamate receptor, metabotropic 4	ENSG00000124493	−1,48	3,08	1,19E-08	6,74E-06
RHOB	Ras homolog family member B	ENSG00000143878	−1,51	1,25	1,21E-06	4,44E-04
ITGAL	Integrin, alpha L (antigen CD11A (p180), lymphocyte function-associated antigen 1; alpha polypeptide)	ENSG00000005844	−1,51	8,58	7,63E-34	8,39E-30
CD52	CD52 molecule	ENSG00000169442	−1,51	6,12	7,33E-20	2,02E-16

(*Continued*)

Table 2 (Continued).

HGNC Symbol	Description	Ensembl ID	logFC	logCPM	Pvalue	FDR
PHLDA1	Pleckstrin homology-like domain, family A, member 1	ENSG00000139289	−1,52	2,58	1,02E-07	4,50E-05
BCL6	B-cell CLL/lymphoma 6	ENSG00000113916	−1,55	4,51	3,79E-13	5,56E-10
ARHGAP31	Rho GTPase activating protein 31	ENSG00000031081	−1,55	4,72	4,25E-13	5,84E-10
KIAA1683	KIAA1683	ENSG00000130518	−1,58	1,78	1,20E-07	5,18E-05
CREB3L3	cAMP responsive element binding protein 3-like 3	ENSG00000060566	−2,09	8,88	2,62E-35	5,76E-31
CNTFR	Ciliary neurotrophic factor receptor	ENSG00000122756	−2,21	2,35	1,99E-10	1,56E-07
ZP1	Zona pellucida glycoprotein 1 (sperm receptor)	ENSG00000149506	−2,24	2,38	3,39E-05	7,17E-03
MARCO	Macrophage receptor with collagenous structure	ENSG00000019169	−2,48	2,50	1,47E-12	1,70E-09
H2AFY2	H2A histone family, member Y2	ENSG00000099284	−2,76	2,52	1,12E-18	2,73E-15
BTN1A1	Butyrophilin, subfamily 1, member A1	ENSG00000124557	−2,86	2,04	2,76E-12	3,04E-09
S100P	S100 calcium binding protein P	ENSG00000163993	−3,15	2,82	5,20E-17	1,04E-13
PTGDR2	Prostaglandin D2 receptor 2	ENSG00000183134	−3,22	3,94	3,60E-25	1,98E-21
AGXT	Alanine-glyoxylate aminotransferase	ENSG00000172482	−4,76	1,43	2,83E-13	4,45E-10

Notes: Green cells: upregulated; orange cells: downregulated.
Abbreviations: CPM, counts per million; ENSG…ID, Gene annotation in Ensembl; FDR, false discovery rate; HGNC, HUGO Gene Nomenclature Committee; ID, identifier; logFC, logarithmic fold change.

number of $CD3^+$ T cells in ventilated patients compared to ECMO patients (Figure 3E) was significantly reduced. Dependent on the required treatment regime, ie, non-ventilated, ventilated or ECMO receiving, $CD4^+$ (Figure 3F) and $CD8^+$ (Figure 3G) cells were lowest in the ventilated patients. Comparing survivors (S) vs non-surviving patients (D), the number of $CD3^+$ (Figure 3H), $CD4^+$ (Figure 3I), or $CD8^+$ T (Figure 3J) cells was not significantly different.

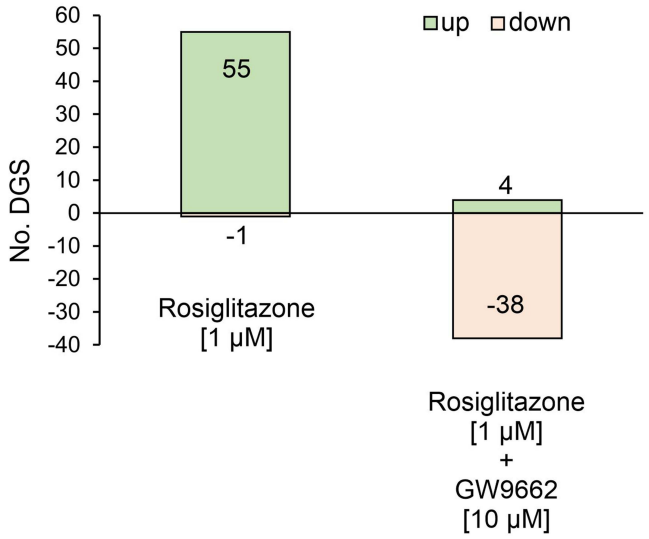

Figure 2 T cell transcriptome in response to PPARγ activation/inhibition. Jurkat T cells were transduced with an inducible Tet-on vector system to express PPARγ in response to doxycycline treatment. Following selection of positive clones, cells were treated with the PPARγ agonist rosiglitazone [1 µM] (left column) or the combination of rosiglitazone [1 µM] and the irreversible PPARγ antagonist GW9662 [10 µM] (right column) for 24 h. Afterwards cells were harvested, and mRNA isolated as described in Materials and Methods. Following preparation of NGS libraries and sequencing, transcriptome analyses revealed and induction of 55 genes and the downregulation of 1 gene in response to rosiglitazone treatment. After rosiglitazone treatment in combination with GW9662 only 4 genes were induced, and 38 genes were downregulated.
Abbreviations: GW9662, 2-chloro-5-nitro-N-phenylbenzamide; NGS, next generation sequencing; PPARγ, peroxisome proliferator-activated receptor γ.

Table 3 Patient Demographics and Clinical Parameters of the COVID-19 Cohort

Parameter	Overall	Not ventilated (NV)	Ventilated (V)	ECMO	p1 NV vs V	p2 NV vs ECMO	p3 V vs ECMO	p4 S vs D
Total	24 (100)	5 (20,8)	12 (50)	7 (29,2)				
Gender, female/male	6 (24)/18 (76)	1 (20)/4 (80)	2 (16.7)/10 (83.3)	1 (14.3)/6 (85.7)	ns	ns	ns	
Age, yr	65.3 (16.5) 25–93	59.8 (12.9) 32–67	55.1 (30.0) 55–93	67.8 (35.5) 25–70	**	ns	*	
Weight (kg)	90.8 (19.7) 45–120	106 (16.73) 80–120	95.1 (20.5) 55–120	91.2 (47.6) 55–93	ns	ns	ns	
ICU stay, d	24 (4–66)	13 (8–24)	30 (4–33)	16 (12–66)	ns	**	**	
Outcome, death	19 (79.2)	2 (40)	11 (91.7)	6 (85.7)	**	**	ns	
Comorbidities								
Arterial hypertension	17 (71)	2 (40)	6 (50)	4 (57.1)	ns	ns	ns	
Diabetes mellitus	5 (21)	2 (40)	3 (25)	5 (71.4)	ns	ns	ns	
Adipositas	6 (25)	4 (80)	5 (41.7)	5 (71.4)	ns	ns	ns	
Bronchial asthma	1 (4)	0 (0)	0 (0)	1 (14.3)				
COPD	1(4)	0 (0)	0 (0)	1 (14.3)				
Laboratory's values								
CRP, mg/dl	1226 (0.96–4420)	496 (0.96–3906)	1352 (44–4420)	1262 (248–3117)	***	***	ns	ns
Leukocyte count, /nl	9.88 (0.23–52.01)	7.93 (0.23–14.95)	11.09 (2.04–52.01)	9.37 (3.63–39.52)	***	***	***	ns
IL-6, pg/mL	188.4 (31.03–788.6)	91.27 (31.03–249.9	223.3 (72.39–788.6)	193.5 (145.5–476.4)	ns	ns	ns	*
PCT, ng/mL	0.67 (0.05–91.5)	0.18 (0.05–1.73)	0.56 (0.06–91.5)	0.84 (0.1–47.9)	ns	**	ns	ns
LDH, U/l	434 (117–1356)	298 (117–889)	418.5 (185–1192)	473 (208–1356)	***	***	ns	ns

Notes: Data are presented as n (%) for categorical variables or median (interquartile range) for continuous variables. Patients' laboratory values are reported as the respective median of the parameter levels obtained during ICU stay. ICU stay was defined as the days from admission to discharge or death. For more information on data collection and analysis, see supplement. p-values comparing two groups were obtained using Fisher`s exact test or One Way ANOVA analysis with Tukey's comparison test. Patients' median laboratory values are presented. *p < 0.05, **p < 0.01, ***p < 0.001. Hospital's central laboratory's threshold levels are CRP: 0.5 mg/dl, leukocyte count: 10.41 /nl, IL-6: 7 pg/mL, PCT: 0.5 ng/mL, LDH: 248 U/l.

Abbreviations: COPD, chronic obstructive pulmonary disease; CRP, C-reactive protein; D, deceased; d, days; ECMO, extracorporeal membrane oxygenation; ICU, intensive care unit; IL-6, interleukin 6; LDH, lactate dehydrogenase; NV, not ventilated; PCT, procalcitonin; S, surviving; U, units; v, ventilated; yr, year.

https://doi.org/10.2147/ITT.S463601 DovePress

Table 4 Demographics of the Healthy Donors

Total	Gender f/m	Age (yr)
12 (100)	7 (58)/5 (42)	27 (24–59)

Notes: Data are presented as n (%) for categorical variables or median (min-max) for continuous variables.
Abbreviations: f, female; m, male; yr, year.

Comparing the survival curves of female and male patients, we found no difference using the Kaplan–Meier model with a Log-rank (Mantel-Cox) test (data not shown).

Additionally, we determined the time course of serum procalcitonin (PCT), IL-6, C-reactive protein (CRP), and lactate dehydrogenase (LDH) in COVID-19 patients for their 30 days ICU stay. Serum PCT was only slightly elevated (Supplementary Figure 7A), when analysing the time course of 30 days. There, only on 8 days the PCT level was

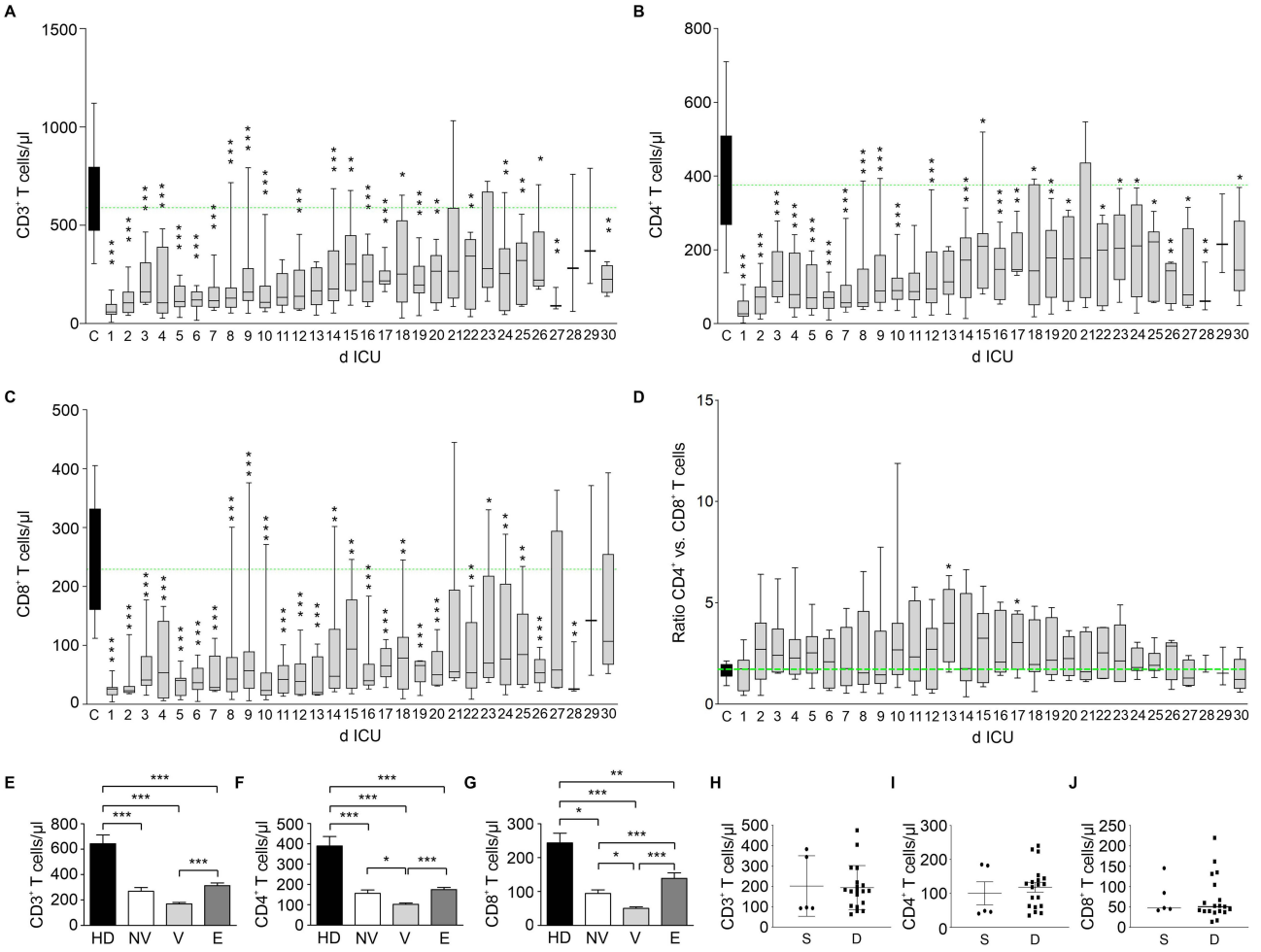

Figure 3 Cell count of $CD3^+$, $CD4^+$, and $CD8^+$ T cells in intensive care COVID-19 patients. Numbers of **(A)** $CD3^+$, **(B)** $CD4^+$, and **(C)** $CD8^+$ T cells as well as **(D)** its ratio ($CD4^+$ vs $CD8^+$) were determined for 30 days intensive care unit stay (d ICU) (n = 24). Cell count/ratio of healthy donors were included as control ((**C**), n = 12 donors). Its median is shown as a green dashed line. To show the impact of the necessary treatment, we compared the cell count of healthy donors (black columns, HD, n = 12 donors) with non-ventilated (white columns, NV, n = 5 patients), ventilated (light grey columns, V, n = 12 patients) and extracorporeal membrane oxygenation (dark grey columns, E, n = 7 patients) requiring patients of **(E)** $CD3^+$, **(F)** $CD4^+$, and **(G)** $CD8^+$ T cells. Finally, we determined the number of **(H)** $CD3^+$, **(I)** $CD4^+$, and **(J)** $CD8^+$ T cells in surviving (S, n = 5 patients) vs deceased (D, n = 19 patients) patients. In **(E)** to **(J)** means were calculated from all samples of the particular patient. These were used to determine the corresponding means, which are shown. *p < 0.05, **p < 0.01, ***p < 0.001.
Abbreviations: C, control; CD, cluster of differentiation; COVID-19, coronavirus disease 2019; D, deceased; E, extracorporeal membrane oxygenation; HD, healthy donors; ICU, intensive care unit; NV, non-ventilated; S, surviving; V, ventilated.

significantly enhanced compared to the hospital's central laboratory's threshold level [0.5 ng/mL] (C), which is shown as a dashed green line. IL-6 expression, with a hospital's central laboratory's threshold level of 7 pg/mL (C, green dashed line), was significantly enhanced over the 30 days ICU stay (Supplementary Figure 7B) which was also true for CRP (Supplementary Figure 7C). Its hospital's central laboratory threshold level is 0.5 mg/dl (C, dashed green line). Finally, the organ damage marker LDH was also increased in COVID-19 patients' sera compared to the hospital's central laboratory's threshold LDH level of 248 U/l (Supplementary Figure 7D, C, green dashed line).

Focusing on the different ventilation strategies required by the COVID-19 patients, we observed highest serum PCT levels in ventilated (V) and ECMO (E) patients, whereas the PCT level was significantly lower in non-ventilated (NV) patients (Supplementary Figure 7E). Analysing these three ventilation settings for IL-6, the lowest IL-6 level was observed in non-ventilated (NV) patients, which is significantly lower than in ventilated (V) or ECMO patients (Supplementary Figure 7F). A similar increase was found for CRP in ventilated (V) and ECMO (E) patients compared to non-ventilated (NV) patients (Supplementary Figure 7G). In non-ventilated (NV) patients' sera LDH was significantly lower compared to ventilated (V) or ECMO (E) patients (Supplementary Figure 7H).

These results are reflected when comparing survivors vs deceased patients. Here, the PCT levels in sera were significantly lower in the survivors (Supplementary Figure 7I). This difference was also found in IL-6, which was significantly higher in the patients who died, compared to those, who survived (Supplementary Figure 7J). However, there was no significant difference in the CRP (Supplementary Figure 7K) and LDH (Supplementary Figure 7L) sera level in surviving (S) vs deceased (D) patients.

Based on previous data, showing an impact of regulatory T cells (T_{reg}) and T_h2 cells in immunosuppression,[36,37] we went on to follow these two $CD4^+$ T cell subpopulations. Thus, we stained for the T_h2 cell marker CRTH2[38,39] and the intracellular T_{reg} indicator FoxP3.[40] In line with our assumption, the number of $CRTH2^+CD4^+$ cells were decreased in COVID-19 patients (Figure 4A). Interestingly, there was no difference in the count of $FoxP3^+CD4^+$ T cells, comparing healthy donors with COVID-19 patients (Figure 4B). Focusing on the different ventilation strategies the patients required, we observed a significant decrease of CRTH2 T cells in non-ventilated (NV) patients (Figure 4C, white vs black column). Ventilated (V) and ECMO receiving patients did not significantly differ in their $CRTH2^+CD4^+$ T cell count compared to healthy donors (HD). However, non-ventilated (NV) patients showed a significant reduced number of $CRTH2^+CD4^+$ T cells compared to ECMO patients (Figure 4C, dark grey vs white column). Concerning FoxP3 expression, we found in healthy donors (HD) a significant higher number of $FoxP3^+CD4^+$ T cells compared to non-ventilated (NV) COVID-19 patients (Figure 4D, black vs white column). Interestingly, the count of $FoxP3^+CD4^+$ T cells was not different in ventilated (V) and ECMO patients compared to healthy donors (HD) (Figure 4D, grey and dark grey vs black column), but was increased significantly compared to non-ventilated (NV) patients (Figure 4D, grey and dark grey vs white column). Finally, we determined the number of $CRTH2^+$ (Figure 4E) and $FoxP3^+CD4^+$ T cells (Figure 4F) on surviving (S) vs non-surviving (D) patients compared to healthy donors. $CRTH2^+CD4^+$ T cells were significantly decreased in surviving (S) patients compared to healthy volunteers (HD) (Figure 4E white vs black column) whereas the $CRTH2^+CD4^+$ T cell count in non-surviving patients was only slightly but not significantly reduced. Concerning the number of $FoxP3^+CD4^+$ T cells, there was a significant reduction in surviving (S) patients compared to healthy donors and deceased patients as well (Figure 4F, white vs black and dark grey column). To also include a relative representation of the cell count, we analysed the percentage of $CRTH2^+$ and $FoxP3^+$ cells of $CD4^+$ T cells in surviving (S) and deceased (D) patients compared to healthy donors (HD) (Supplementary Figure 8). The percentage of $CRTH2^+$ of $CD4^+$ T cells was increased in COVID-19 patients, independent of whether they died or survived (Supplementary Figure 8A). There was no difference in the percentage of $CRTH2^+$ of $CD4^+$ T cells in female vs male patients (Supplementary Figure 8B). Analysing the percentage of $FoxP3^+$ of $CD4^+$ T cells, we found a significant increase in patients who died, compared to healthy donors (Supplementary Figure 8C). This was validated for the male part of the patients/donors showing a significant increase in the percentage of $FoxP3^+$ cells only in male patients, who died, compared to healthy donors (Supplementary Figure 8D).

Considering cell death as possible mechanism causing T cell depletion in COVID-19 patients, we analysed apoptotic and necrotic cells. Strikingly, cell death, ie the number of apoptotic and necrotic $CD3^+$ cells, was not altered in blood samples of COVID-19 patients compared to healthy volunteers (Supplementary Figure 9).

In some analogy to the sepsis patients, where PPARγ mRNA expression in T cells was associated with a low number of T cells and a worse outcome,[19] we stained intracellularly for PPARγ protein in advance to our already published data analysing PPARγ

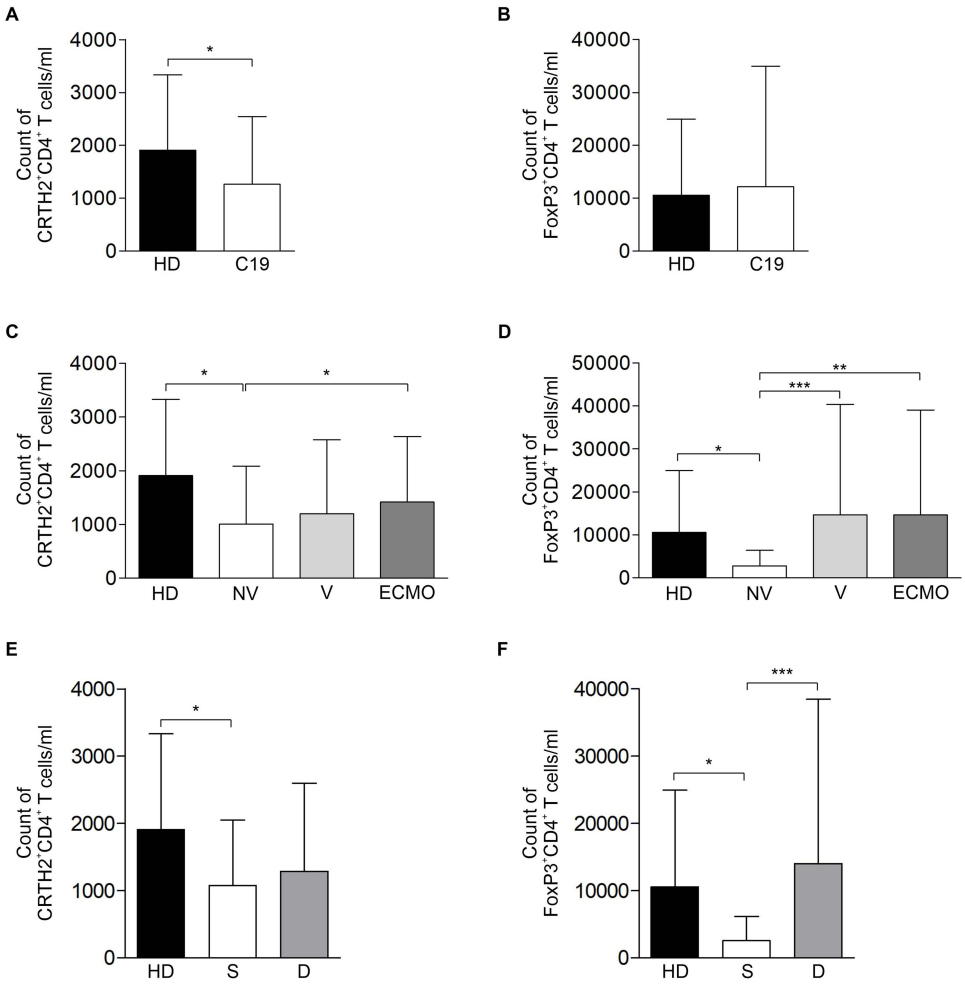

Figure 4 T_h2 cells and regulatory T cells (T_{reg}) in the blood of intensive care COVID-19 patients. The chemoattractant receptor-homologous molecule expressed on T_h2 cells (CRTH2) surface marker was stained **(A)** to determine T_h2 cell count in COVID-19 patients (C19, n = 24 patients) compared to healthy donors (HD, n = 12 donors). FoxP3 was intracellularly detected **(B)** as a T_{reg} marker comparing COVID-19 patients (C19, n = 24 patients) and healthy donors (HD, n = 12 donors). To show the effect of different ventilation regimes on the expression of CRTH2 and FoxP3, we compared the number of **(C)** $CRTH2^+$ or **(D)** $FoxP3^+$ with the count found in non-ventilated (white columns, NV, n = 5 patients), ventilated (light grey columns, V, n = 12 patients), and extracorporeal membrane oxygenation requiring patients (dark grey columns, ECMO, n = 7 patients). Finally, we checked the count of **(E)** $CRTH2^+$ and **(F)** $FoxP3^+$ T cells of COVID-19 patients, who survived (S, n = 5 patients) against deceased patients (D, n = 19 patients) compared to healthy donors (HD, n = 12 patients). Means calculated from all samples of the particular patients were used to determine the corresponding means, which are shown. All values are presented as cells/mL peripheral blood. *p < 0.05, **p < 0.01, ***p < 0.001.

Abbreviations: C-19, COVID-19 patients; COVID-19, coronavirus disease 2019; CRTH2, chemokine receptor homologue expressed on T_h2 cells; D, deceased; ECMO, extracorporeal membrane oxygenation; FoxP3, forkhead box protein 3; HD, healthy donors; NV, non-ventilated; S, survived; T_h2, T helper cells type 2; T_{reg}, regulatory T cells; V, ventilated.

mRNA expression by qPCR[19] or protein expression by Western blotting.[41] As depicted in Figure 5A, left part, we found an increased PPARγ expression in $CD4^+$ T cells of intensive care COVID-19 patients, which was blocked using the unlabelled PPARγ antibody as a specific competitor (Figure 5A, middle panel), whereas an unspecific antibody did not alter PPARγ antibody binding (Figure 5A, right panel). Quantification (Figure 5B) of FACS data revealed a statistically significant increase in PPARγ expression of roughly 1.6-fold (Figure 5B, healthy donors mean fluorescence 520.3 ± 13.17; COVID-19 patients mean fluorescence 838.8 ± 77.03; *p > 0.05). Based on these data, we were encouraged to determine the role of the PPARγ target gene CRTH2 in HEK293T cells.

Overexpression of the PPARγ Target Gene CRTH2 Sensitized Towards PPARγ Activation

Thus, we determined whether CRTH2 overexpression in HEK293T cells was associated with an increased PPARγ transactivation following treatment of cells with 15d-PGJ_2, putatively connected to an increased rate of cell death. Having verified expression of CRTH2 in the transiently transfected HEK293T cells, these cells were transiently transfected with a PPARγ expression vector in combination with a reporter vector containing three PPREs followed by

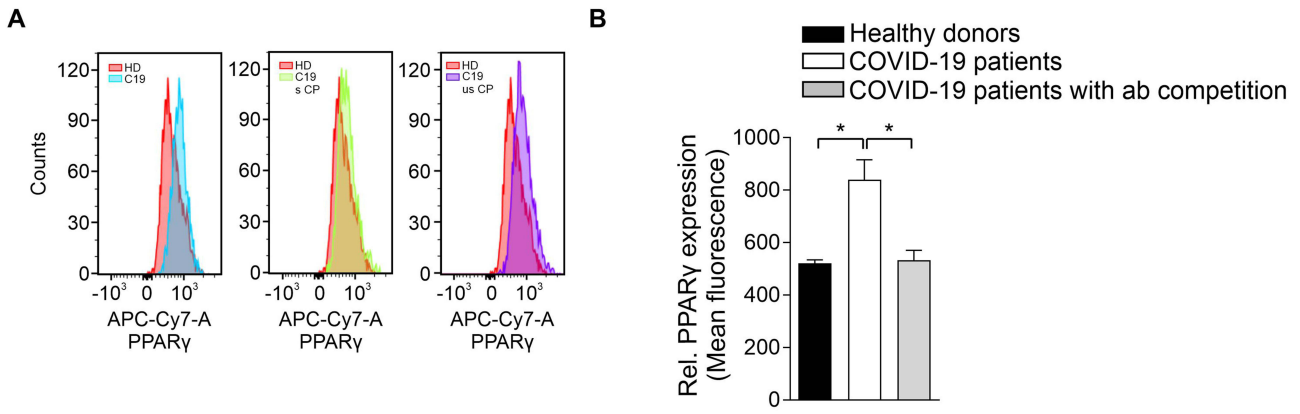

Figure 5 PPARγ expression in $CD4^+$ T cells derived from intensive care COVID-19 patients. **(A)** Leukocytes were isolated from blood by erythrocyte lysis. $CD4^+$ T cells were stained with an AmCyan-labeled anti-CD4 antibody and intracellular PPARγ was detected following the protocol for FoxP3 staining using an AlexaFluor750-labeled-anti -PPARγ antibody (left panel; HD, healthy donor; C19, COVID-19 patient). As a control, the PPARγ antibody was included unlabeled 1:10 to the labeled antibody to show specific binding (middle panel; HD, healthy donor; C19, COVID-19 patient; s CP, specific competition). An unspecific antibody (anti-FoxP3-APC), used 1:10, was included as well (right panel: HD, healthy donor; C19, COVID-19 patient; us CP, unspecific competition). **(B)** Quantification of the relative PPARγ expression (mean fluorescence ± SE) of healthy donors (black bar) compared to intensive care COVID-19 patients (white bar). Unlabeled PPARγ antibody competition was included to show PPARγ-binding specificity (grey bar, n = 5). Samples of the patients were drawn on the first or second day during the ICU stay. *p < 0.05.

Abbreviations: A, area; APC, allophycocyanin; APC-Cy7, APC-cyanine 7; C19, COVID-19 patient; CD, cluster of differentiation; COVID-19, corona disease 2019; FoxP3, forkhead box protein 3; HD, healthy donor; PPARγ, peroxisome proliferator-activated receptor γ; s CP, specific competition; SE, standard error; us CP, unspecific competition.

a thymidine kinase promoter in front of a firefly luciferase gene. As shown in Figure 6A, 15d-PGJ_2 concentration-dependently induced PPARγ transactivation in CRTH2-overexpressing HEK293T cells significantly more than in EGFP expressing control cells. 15d-PGJ_2-dependent PPARγ transactivation was prevented in CRTH2-overexpressing HEK293T cells by the pre-incubation of the cells for 30 min with the CRTH2 antagonist fevipiprant before 15d-PGJ_2 addition (Figure 6B). In contrast, treatment with 10 µM rosiglitazone, a PPARγ agonist, provoked a similar PPARγ-dependent transactivation in CRTH2-overexpressing cells compared to EGFP-control cells (Figure 6B). To verify a role of PPARγ, the transient transfection of a d/n PPARγ mutant, not allowing ligand binding, significantly reduced 15d-PGJ_2 induced PPARγ transactivation (Supplementary Figure 10) in CRTH2-overexpressing HEK293T cells.

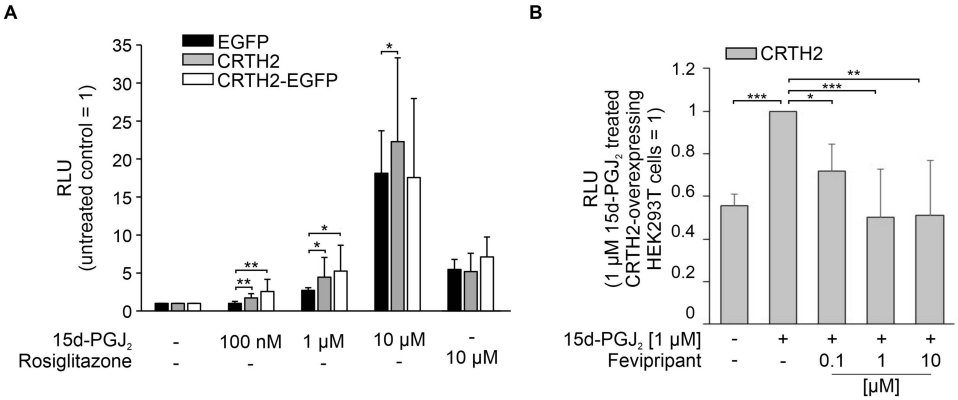

Figure 6 CRTH2 overexpression enhanced 15-deoxy-Δ12,14-prostaglandin J_2 (15d-PGJ_2)-dependent PPARγ activation in HEK293T cells. **(A)** CRTH2 expression vectors encoding for CRTH2 (grey column), CRTH2-EGFP (white column) or EGFP (black column) were transiently transfected into HEK293T cells in combination with a PPRE-containing PPARγ reporter plasmid and a renilla-firefly luciferase encoding control vector. Transfected cells were treated with 100 nM, 1 µM or 10 µM 15d-PGJ_2 or 10 µM rosiglitazone (PPARγ agonist). PPARγ-dependent transactivation was followed as relative luciferase units (RLU), which is the quotient from PPRE-driven firefly-luciferase activity by the CMV-induced renilla luciferase activity as transfection efficiency control, normalized to the untreated controls (= 1) (n = 6–11). **(B)** HEK293T cells transiently transfected with a CRTH2 expression vector and the PPARγ reporter system as described in (**A**), were treated with 1 µM 15d-PGJ_2 and 100 nM, 1 µM, or 10 µM of the CRTH2 inhibitor fevipripant or remained untreated as a control. PPARγ transactivation was determined as in (**A**) (n = 4–7). *p < 0.05, **p < 0.01, ***p < 0.001.

Abbreviations: 15d-PGJ_2, 15-deoxy-Δ12,14-prostaglandin J_2; CMV, cytomegalovirus; CRTH2, chemokine receptor homologue expressed on T_h2 cells; EGFP, enhanced green fluorescent protein; PPARγ, peroxisome proliferator activate receptor γ; PPRE, peroxisome proliferator responsive element; RLU, relative luciferase units.

Overexpression of CRTH2 Did Not Sensitize Towards 15d-PGJ$_2$-Dependent Apoptosis

Considering PPARγ expression as a pro-apoptotic marker as observed in T cells derived from sepsis patients,[13,19] we determined whether sensitizing cells to PPARγ-dependent transactivation by CRTH2 overexpression is also associated with apoptosis in Jurkat T cells. Using Jurkat T cells, which have been stably transduced with a CRTH2 encoding vector or a CRTH2-EGFP vector, or wild type Jurkat T cells (Supplementary Figure 11), there was no difference in cell death, following 15d-PGJ$_2$ treatment. 100 nM and 1 µM 15d-PGJ$_2$ neither increased cell death in CRTH2 overexpressing Jurkat cells nor in Jurkat control cells. In contrast, 10 µM 15-d-PGJ$_2$ significantly induced apoptosis in all three Jurkat clones independently from CRTH2 overexpression (Supplementary Figure 12A). A quantification is presented in Supplementary Figure 12B.

T$_h$2-Differentiation is Associated with CRTH2 Expression

To verify cell culture data from Jurkat T cells in primary T cells, we isolated CD4$^+$ T cells from blood derived from healthy donors. Intracellular staining of marker cytokines of T$_h$1 (IFN-γ) and T$_h$2 (IL-4) cells revealed that the number of IL-4-positive cells before T$_h$2 differentiation was roughly 43.2 ± 10.6 cells, whereas IFN-γ-positive cells were approximately 1.8 ± 1.3 cells (Figure 7A), which means 24-fold more IL-4-positive cells compared to IFN-γ-positive-cells. After 13 days T$_h$2 differentiation, the count of IL-4-positive cells was increased to 5692 ± 4374. The number of IFN-γ -positive T cells also increased to untreated cells (93.8 ± 60.2) (Figure 7B). The ratio of IL-4-positive to IFN-γ-positive CD4 T cells increased to 60-fold more IL-4-positive cells. Undifferentiated and differentiated T$_h$2 cells were stimulated for

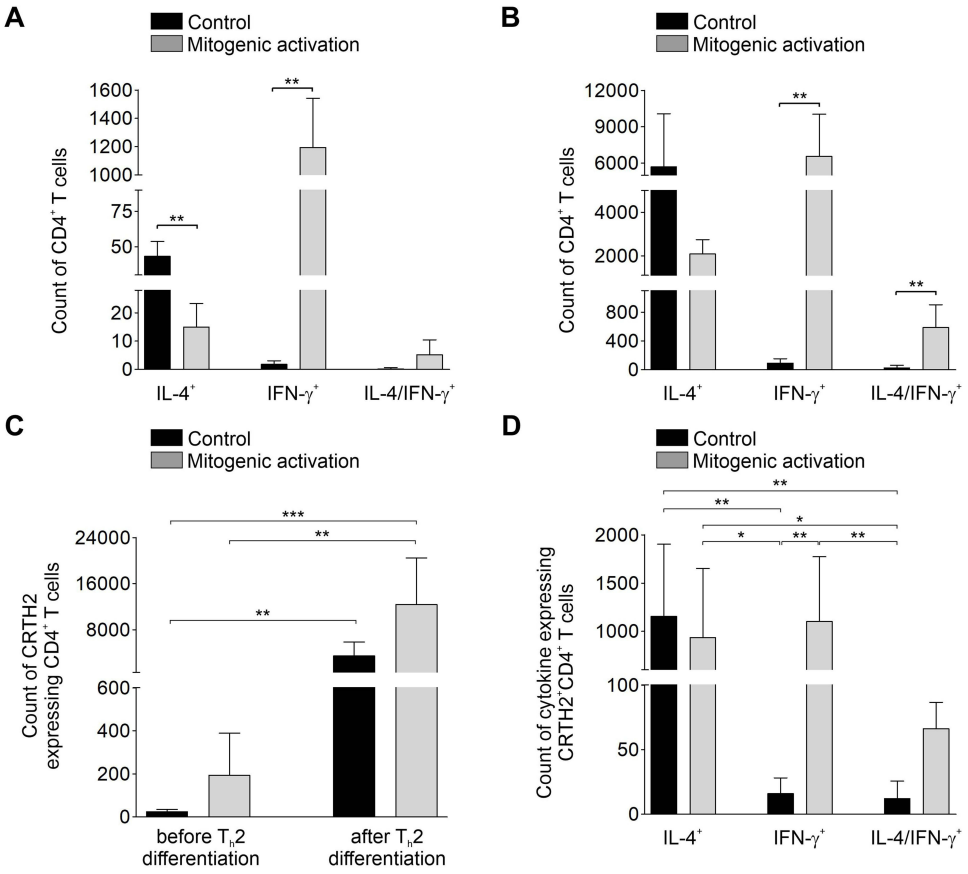

Figure 7 Differentiation of blood derived primary CD4$^+$ T cells to T$_h$2 cells. CD4$^+$ T cells were enriched from blood of healthy donors by positive isolation using the MACS based technology. CD4$^+$ T cells were differentiated for 13 days as described in Materials and Methods. To determine the effect of T$_h$2 differentiation on blood derived CD4$^+$ cells, CD4$^+$ cells were analysed for intracellular expression of the T$_h$2 marker IL-4 and the T$_h$1 marker IFN-γ before **(A)** (n = 5) and after **(B)** (n = 6) differentiation, with (grey columns) or without (black columns) an additional mitogenic activation for 6 h. The same treatment was performed to analyze **(C)** CRTH2 expression before (n = 5) and following T$_h$2 differentiation (n = 6). **(D)** Co-expression of CRTH2, IL-4, and/or IFN-γ was determined only after T$_h$2 differentiation (n = 6). * p < 0.05, **p < 0.01, ***p < 0.001.

Abbreviations: CD, cluster of differentiation; CRTH2, chemokine receptor homologue expressed on T$_h$2 cells; IFN-γ, interferon-γ; IL-4, interleukin-4; MACS, magnetic cell separation; T$_h$1, T helper cells type 1; T$_h$2, T helper cells type 2.

6 h with a cell activation cocktail, containing phorbol 12-myristate 13-acetate (PMA), and ionomycin to activate the T cells. The activation cocktail already contained monensin to prevent cytokine release from the cells. Considering different requirements of cytokines to be effectively retained in the cell,[33] we added BD GolgiPlug™, containing brefeldin A as well. This treatment led to 1194 ± 347.2 IFN-γ-positive $CD4^+$ T cells before T_h2 differentiation, which was increased to 6553 ± 3481 after T_h2 differentiation. To the contrary, this mitogenic stimulation reduced the count of IL-4-positive $CD4^+$ T cells to 15 ± 8.1 in undifferentiated $CD4^+$ T cells (Figure 7A) and to 2085 ± 658.7 IL-4-positive $CD4^+$ T cells following 13 days T_h2 differentiation (Figure 7B). Interestingly, we found also $CD4^+$ T cells positive for IL-4 and IFN-γ in parallel. Although CRTH2 has been established as an T_h2 marker receptor,[39] we were interested to determine co-expression of IL-4 and CRTH2 as well as IFN-γ in $CD4^+$ T cells. Thus, we found that the number of CRTH2-positive $CD4^+$ T cells is also increased following T_h2 differentiation (24 ± 10.84 vs 3484 ± 2404, Figure 7C, black columns) similarly to the rise of IL-4 expressing cells compared to undifferentiated cells. Interestingly, the number of $CRTH2^+$ T cells was enhanced in response to T cell activation before and following T_h2 differentiation (193 ± 196 vs 12391 ± 8062, Figure 7C, grey columns). Analysing whether CRTH2-positive $CD4^+$ T cells co-express IL-4 and/or IFN-γ, we found that following T_h2 differentiation 1153 ± 750.9 $CRTH2^+CD4^+$ T cells co-express IL-4 (Figure 7D, first black column), whereas only 16 ± 12.1 $CRTH2^+CD4^+$ expressing cells co-express IFN-γ (Figure 7D, second black column). T cell activation provoked a reversal of this induction. The count of $CRTH2^+CD4^+$ T cells co-expressing IL-4 was slightly reduced to 933.5 ± 718.7 (Figure 7D, first grey column), and the number of IFN-γ-positive cells was significantly increased to 1101 ± 672.2 (Figure 7D, second grey column). The number of $CRTH2^+CD4^+$ cells co-expressing IL-4 and IFN-γ as well was not significantly altered (12.2 ± 13.5 vs 66.3 ± 20.3) (Figure 7D, third grey and black columns).

To get a first hint for a role of PPARγ in T_h2 differentiation of primary T cells, we treated cells with the PPARγ antagonist GW9662 during the T_h2 differentiation regime as shown in Supplementary Figure 13. 10 μM GW9662 added in parallel to the T_h2 differentiation cocktail did not change the number of IL-4 expressing $CD4^+$ cells (Supplementary Figure 13A), whereas the count of CTRH2 expressing $CD4^+$ T cells was significantly reduced (Supplementary Figure 13B).

Pro-Apoptotic Role of CRTH2 Expression in Primary T_h2 Cells

Based on our results, we hypothesized that CRTH2 may sensitize primary $CD4^+$ T cells towards apoptosis. To test this assumption, we determined cell death in $CD4^+$ T cells directly following T_h2 differentiation (Figure 8). Whereas all $CD4^+$ T cells showed a viability of roughly 80% (Figure 8A), dividing these cells into $CRTH2^+$ and $CRTH2^-$ interestingly demonstrated that $CRTH2^+$ cells were prone to cell death, only remaining 20% of cells viable (Figure 8B), whereas in $CRTH2^-$ T cells, cell death was not increased (Figure 8C). The quantification of these data (Figure 8D) further supported the assumption that primary $CRTH2^+CD4^+$ T cells are sensitized towards cell death.

Further studies will prove whether PPARγ is involved in cell death of $CRTH2^+$ $CD4^+$ T cells in COVID-19 patients.

Discussion

Up to now (status 10th March 2023, coronavirus.jhu.edu/map.html) COVID-19 has provoked worldwide roughly 676.6 million positive infections, with a mortality of 6.88 million. For therapeutic approaches in patients diseased with COVID-19, it is important to understand the key pathophysiological principles leading to this infectious disease. This is also true for biomarkers, which allow the classification of pro- vs anti-inflammatory or hyper- vs hypo-inflammatory responses, implying the state of the disease,[42,43] including starting points for personalized medicine approaches.[44] In COVID-19 patients, T cell exhaustion[45] and inhibition of T cells responses during the acute phase have already been described.[46] We focused our interest on the nuclear receptor PPARγ. This ligand-dependent transcription factor is known to be expressed in activated but not resting T cells.[13,14,16] Its activation is associated with T cell death.[8,13,19] This is in line with our previous reports, where we observed PPARγ-mRNA expression in T cells derived from sepsis patients[16,19] and correlated a low blood T cell count with high PPARγ expression and a worse outcome.[19] To determine, whether the number of T cells also is reduced in intensive care COVID-19 patients, we stained T cells derived from patients´ blood for the expression of surface markers CD3, CD4, and CD8 and additionally for CRTH2, a surface marker of T_h2 cells, identified as a putative PPARγ target gene in this study. Moreover, we analysed intracellular expression of the T_{reg} marker transcription factor FoxP3 and PPARγ with its specific consideration of a key regulator in apoptosis of activated T cells during sepsis.[16] In line with our assumption, originating from the sepsis

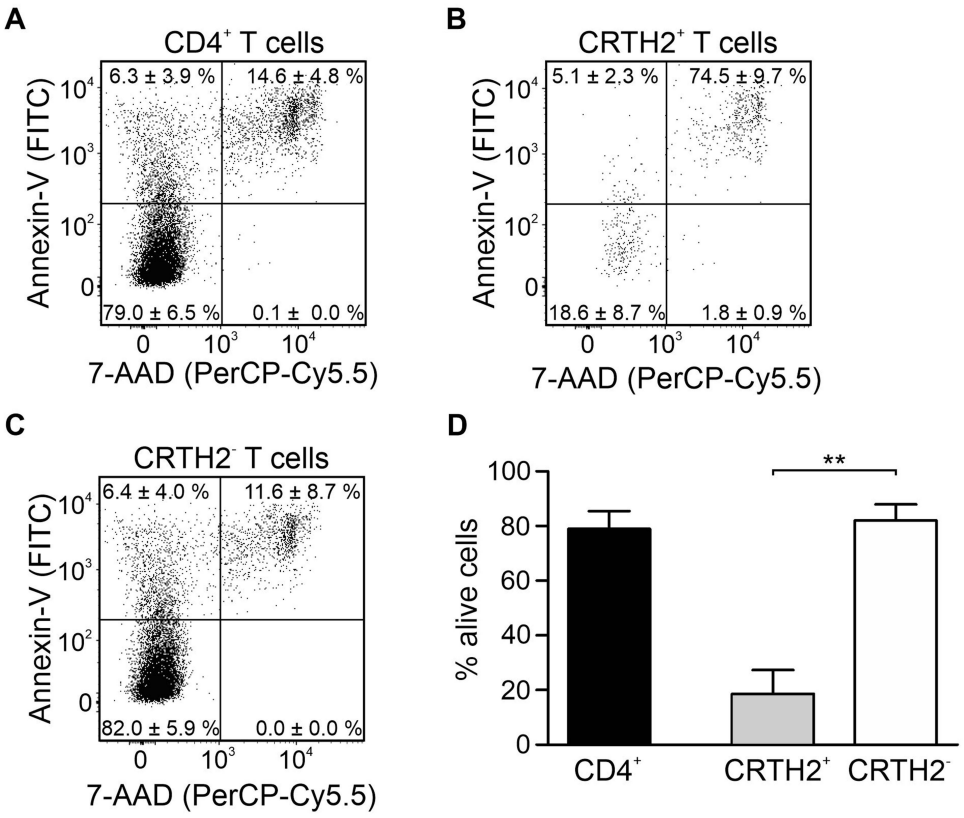

Figure 8 CRTH2$^+$ primary CD4$^+$ T cells are associated with cell death. Following T_h2 differentiation, cell death was analyzed in (**A**) CD4$^+$ T cells, (**B**) CRTH2$^+$ T cells, and (**C**) CRTH2$^-$ T cells. Apoptosis was detected by annexin-V staining and necrosis was followed by 7-aminoactinomycin D (7-AAD). Quantification of these data is shown in (**D**) (n = 4). **p < 0.01.
Abbreviations: 7-AAD, 7-aminoactinomycin D; CD, cluster of differentiation; CRTH2, chemokine receptor homologue expressed on T_h2 cells; T_h2, T helper cells type 2.

patients, we observed a reduced T cell count in intensive care COVID-19 patients. In the acute phase of a COVID-19 infection, the number of CD3$^+$, CD4$^+$, and CD8$^+$ T cells in the blood of intensive care patients was reduced, which is similar to sepsis.[42] Considering the newly identified PPARγ target gene CRTH2 in T cells, we observed a shift from T_h1 to T_h2 cells in COVID-19 patients. This phenotype shift compromised most likely also the anti-viral immune response. Interestingly, a shift of the pro-inflammatory T_h1 response, characterized by the release of IFN-γ, to an anti-inflammatory, resolution promoting T_h2 phenotype associated with IL-4 synthesis, also reduces the immune response and thus, contributes to an inadequate immune defence.[47,48]

Our results are supported by the data of Gil-Etayo et al[49,50] showing that a favored T_h1 response in COVID-19 patients is an independent protective factor for the prevention of hospitalization, consequently often associated with an asymptomatic SARS-COV-2 infection.[50] In line with this, the authors observed a significant reduction of %T_h1 and %T_h17 cells with higher activated %T_h2 cells in hospitalized COVID-19 patients compared to healthy controls.[49] Moreover, the percentage of senescent T_h2 cells was higher in severe COVID-19 patients who died compared to those who survived.[49]

Recently, in the literature, a dual role of CRTH2 in acute lung injury (ALI) has been suggested.[51] Expressed only on neutrophils, which have been extravasated to the lung, the pharmacological CRTH2 inhibition with fevipiprant reduced reactive oxygen formation by neutrophils in vitro. In line with this, CRTH2 activation by its specific agonist 13.14-dihydro-15-keto-PGD_2 (DK-PGD_2) provoked an inflammatory response.[51] On the other hand, CRTH2-deficient mice showed a worsening of lung injury in an LPS model of ALI. These data indicate that CRTH2 is involved in neutrophil activation and in mediating a more resolving type 2 immune response.

Considering the impact of T_h2 cells in the resolution of inflammation, an increase of T_h1 to T_h2 cells might contribute to COVID-19 severity including disease chronification. These data are supported by the study of Roncati et al, showing that on blood smears of intensive care patients, T_h2 cell markers were increased.[37] Additionally, the count of FoxP3-positive regulatory T cells (T_{reg}) increased.[36] Based on this T cell depletion and bias of T cell phenotypes, the anti-viral

immunity was significantly reduced. This shift might be caused by oxidative stress, originating from the immune response or following the release of damage-associated molecular pattern (DAMP)[52] such as reactive carbonyls[53] or HMGB1 as shown in our previous data.[54] Diagnostic findings from COVD-19 patients point to the importance of T_h1 and cytotoxic T cells in mediating the anti-viral response.[37] Correspondingly, a T cell phenotype shift to T_h2, impairs an adequate fight against the infection.[55] However, a T_h1 to T_h2 phenotype shift has also been described by the activation of the ligand-dependent transcription factor PPARγ without analysing its target genes.[56,57]

Recent data have identified a different role of PPARγ in B cells.[58] There, independently from its role as a transcription factor, PPARγ has been identified to mediate the degradation of phosphorylated STAT6 as an E3-ubiquitin ligase, inhibiting IgE synthesis during asthma.[58] These data provide a new function of PPARγ, which has not been analysed in T cells.

Interestingly, the endogenous PPARγ ligand 15-d-PGJ_2, which belongs to the cyclopentone prostaglandins, has also been shown to have anti-viral activity against RNA viruses.[59,60] In some analogy, it has been proposed that a CRTH2 antagonist in combination with a TXA_2 antagonist might be associated with a boost of IFN-λ in the upper respiratory tract. This consequently is associated with a limited SARS-CoV-2 replication and transmission.[61–63] Moreover, in a lethal influenza mouse model, treatment of the animals with 15d-PGJ_2 improved survival and reduced lung inflammation.[64] These contrary results to our COVID-19 data significantly show the importance of the time point of 15d-PGJ_2 treatment/synthesis. This is further fostered by the observation, that in the mouse model treatment with 15d-PGJ_2 was only effective when given 1 day following the infection whereas it was ineffective when given in parallel with the infection. This time dependency is also valid, when antagonizing PPARγ in a polymicrobial murine cecal-ligation and puncture model to improve survival.[8] Considering this time-based outcome, the use of appropriate PPARγ modulators, leading to its activation or inhibition, first require the expression of PPARγ in the target cell(s) and second, the knowledge of the need, whether an anti-inflammatory or an anti-apoptotic effect is required.

Conclusion

In conclusion, the data of our pilot study in intensive care COVID-19 patients, suggests that PPARγ is involved in T cell apoptosis and T_h2 differentiation of T cells. Our results, that CRTH2 expression sensitizes T cells to cell death, putatively by enhancing PPARγ activation, are supported by data obtained from COVID-19 patients, showing an enhanced release of PGD_2 and its derivative 15-dPGJ_2.[65–67] This is also found in murine COVID-19 models, where synthesis of PGD_2 and expression of its receptor CRTH2 were age-dependently increased.[68]

Therefore, this should be considered as basic concept for further study as a possible therapeutic concept. It is obvious to continue the analyses of mechanisms, which are important to change the phenotype of T cells to T_h2 or T_{reg} cells or to kill T cells, and consequently all dampen the immune response.

Data Sharing Statement

Data are available on request from the corresponding author.

Ethical Approval

The study was performed in accordance with the Declaration of Helsinki. Approval from the local ethics committee was obtained before the study was conducted (reference #20-643, #20-982) and a waiver regarding the requirement of written informed consent from COVID-19 patients was authorized. All participants of the control group provided written informed consent.

Author Contributions

All authors made a significant contribution to the work reported, whether that is in the conception, study design, execution, acquisition of data, analysis and interpretation, or in all these areas; took part in drafting, revising or critically reviewing the article; gave final approval of the version to be published; have agreed on the journal to which the article has been submitted; and agree to be accountable for all aspects of the work.

Disclosure

The Department of Anesthesiology, Intensive Care Medicine & Pain Therapy of the University Hospital Frankfurt, Goethe University received support from B. Braun Melsungen, CSL Behring, Fresenius Kabi, and Vifor Pharma for the implementation of Frankfurt's Patient Blood Management program. K.Z. has received honoraria for participation in advisory board meetings for Haemonetics and Vifor and received speaker fees from CSL Behring, Masimo, Pharmacosmos, Boston Scientific, Salus, iSEP, Edwards and GE Healthcare. He is the Principal Investigator of the EU-Horizon 2020 project ENVISION (Intelligent plug-and-play digital tool for real-time surveillance of COVID-19 patients and smart decision-making in Intensive Care Units) and Horizon Europe 2021 project COVend (Biomarker and AI-supported FX06 therapy to prevent progression from mild and moderate to severe stages of COVID-19). M.J.P is currently an employee of EpiEndo Pharmaceuticals ehf. Iceland, personal fees from Phialogics AG, outside the submitted work; In addition, M.J.P. has a patent WO2016/012312 A1 issued. H.N. reports personal fees from Biotest AG, personal fees from Pfizer, outside the submitted. K.S. reports being the Co-founder of Noscendo GmbH, outside the submitted work; In addition, K.S. has a patent US10910088B2 issued. The authors report no other conflicts of interest in this work.

References

1. Gaieski DF, Edwards JM, Kallan MJ, Carr BG. Benchmarking the incidence and mortality of severe sepsis in the United States. *Crit Care Med*. 2013;41(5):1167–1174. doi:10.1097/ccm.0b013e31827c09f8
2. Angus DC, van der Poll T. Severe sepsis and septic shock. *N Engl J Med*. 2013;369(9):840–851. doi:10.1056/nejmra1208623
3. Mehta P, Porter JC, Manson JJ, et al. Therapeutic blockade of granulocyte macrophage colony-stimulating factor in COVID-19-associated hyperinflammation: challenges and opportunities. *Lancet Respir Med*. 2020;8(8):822–830. doi:10.1016/s2213-2600(20)30267-8
4. Brady J, Horie S, Laffey JG. Role of the adaptive immune response in sepsis. *Intensiv Care Med Exp*. 2020;8(Suppl 1):20. doi:10.1186/s40635-020-00309-z
5. Rittirsch D, Flierl MA, Ward PA. Harmful molecular mechanisms in sepsis. *Nat Rev Immunol*. 2008;8(10):776–787. doi:10.1038/nri2402
6. Hotchkiss RS, Nicholson DW. Apoptosis and caspases regulate death and inflammation in sepsis. *Nat Rev Immunol*. 2006;6(11):813–822. doi:10.1038/nri1943
7. Hotchkiss RS, Karl IE. The pathophysiology and treatment of sepsis. *N Engl J Med*. 2003;348(2):138–150. doi:10.1056/nejmra021333
8. Schmidt MV, Paulus P, Kuhn AM, et al. Peroxisome proliferator–activated Receptor γ–induced T cell apoptosis reduces survival during polymicrobial sepsis. *Am J Respir Crit Care Med*. 2011;184(1):64–74. doi:10.1164/rccm.201010-1585oc
9. Hernandez-Olmos V, Knape T, Heering J, et al. Structure optimization of a new class of PPARγ antagonists. *Bioorg Med Chem*. 2019;27(21):115082. doi:10.1016/j.bmc.2019.115082
10. Knape T, Flesch D, Kuchler L, et al. Identification and characterisation of a prototype for a new class of competitive PPARγ antagonists. *Eur J Pharmacol*. 2015;755:16–26. doi:10.1016/j.ejphar.2015.02.034
11. Knape T, Hernandez-Olmos V, Flesch D, et al. Improved selective peroxisome proliferator activated receptor gamma modulators (SPPARγMs). *Intensiv Care Med Exp*. 2018;6(Suppl 1):1–33. doi:10.1186/s40635-018-0196-z
12. von Knethen A, Sha LK, Knape T, et al. Activation of the peroxisome proliferator-activated receptor γ counteracts sepsis-induced T cell cytotoxicity toward alloantigenic target cells. *J Mol Med*. 2015;93(6):633–644. doi:10.1007/s00109-014-1249-8
13. Tautenhahn A, Brüne B, von Knethen A. Activation-induced PPARγ expression sensitizes primary human T cells toward apoptosis. *J Leukoc Biol*. 2003;73(5):665–672. doi:10.1189/jlb.1002487
14. Wang YL, Frauwirth KA, Rangwala SM, Lazar MA, Thompson CB. Thiazolidinedione activation of peroxisome proliferator-activated receptor γ can enhance mitochondrial potential and promote cell survival. *J Biol Chem*. 2002;277(35):31781–31788. doi:10.1074/jbc.m204279200
15. Harris SG, Phipps RP. The nuclear receptor PPAR gamma is expressed by mouse T lymphocytes and PPAR gamma agonists induce apoptosis. *Eur J Immunol*. 2001;31(4):1098–1105. doi:10.1002/1521-4141(200104)31:4<1098::aid-immu1098>3.0.co;2-i
16. Soller M, Tautenhahn A, Brüne B, et al. Peroxisome proliferator-activated receptor γ contributes to T lymphocyte apoptosis during sepsis. *J Leukoc Biol*. 2006;79(1):235–243. doi:10.1189/jlb.0205058
17. Scher JU, Pillinger MH. 15d-PGJ2: the anti-inflammatory prostaglandin? *Clin Immunol*. 2005;114(2):100–109. doi:10.1016/j.clim.2004.09.008
18. Surh YJ, Na HK, Park JM, et al. 15-Deoxy-Δ12,14-prostaglandin J2, an electrophilic lipid mediator of anti-inflammatory and pro-resolving signaling. *Biochem Pharmacol*. 2011;82(10):1335–1351. doi:10.1016/j.bcp.2011.07.100
19. Brenneis M, Aghajaanpour R, Knape T, et al. Pparγ expression in T cells as a prognostic marker of sepsis. *SHOCK*. 2016;45(6):591–597. doi:10.1097/shk.0000000000000568
20. Patel L, Pass I, Coxon P, Downes CP, Smith SA, Macphee CH. Tumor suppressor and anti-inflammatory actions of PPARγ agonists are mediated via upregulation of PTEN. *Curr Biol*. 2001;11(10):764–768. doi:10.1016/s0960-9822(01)00225-1
21. Yang XY, Wang LH, Chen T, et al. Activation of human T lymphocytes is inhibited by peroxisome proliferator-activated receptor γ (PPARγ) agonists PPARγ co-association with transcription factor NFAT. *J Biol Chem*. 2000;275(7):4541–4544. doi:10.1074/jbc.275.7.4541
22. Trümper V, Wittig I, Heidler J, Richter F, Brüne B, von Knethen A. Redox regulation of PPARγ in polarized macrophages. *PPAR Res*. 2020;2020:8253831. doi:10.1155/2020/8253831
23. Leesnitzer LM, Parks DJ, Bledsoe RK, et al. Functional consequences of cysteine modification in the ligand binding sites of peroxisome proliferator activated receptors by GW9662. *Biochemistry*. 2002;41(21):6640–6650. doi:10.1021/bi0159581
24. Lehmann JM, Moore LB, Smith-Oliver TA, Wilkison WO, Willson TM, Kliewer SA. An antidiabetic thiazolidinedione is a high affinity ligand for peroxisome proliferator-activated receptor γ (PPARγ)*. *J Biol Chem*. 1995;270(22):12953–12956. doi:10.1074/jbc.270.22.12953

25. Forman BM, Tontonoz P, Chen J, Brun RP, Spiegelman BM, Evans RM. 15-Deoxy-Δ12,14-Prostaglandin J2 is a ligand for the adipocyte determination factor PPARγ. *Cell*. 1995;83(5):803–812. doi:10.1016/0092-8674(95)90193-0
26. Abraham RT, Weiss A. Jurkat T cells and development of the T-cell receptor signalling paradigm. *Nat Rev Immunol*. 2004;4(4):301–308. doi:10.1038/nri1330
27. Lin YC, Boone M, Meuris L, et al. Genome dynamics of the human embryonic kidney 293 lineage in response to cell biology manipulations. *Nat Commun*. 2014;5(1):4767. doi:10.1038/ncomms5767
28. Mortazavi A, Williams BA, McCue K, Schaeffer L, Wold B. Mapping and quantifying mammalian transcriptomes by RNA-Seq. *Nat Methods*. 2008;5(7):621–628. doi:10.1038/nmeth.1226
29. Wang L, Wang S, Li W. RSeQC: quality control of RNA-seq experiments. *Bioinformatics*. 2012;28(16):2184–2185. doi:10.1093/bioinformatics/bts356
30. Robinson MD, McCarthy DJ, Smyth GK. edgeR: a Bioconductor package for differential expression analysis of digital gene expression data. *Bioinformatics*. 2010;26(1):139–140. doi:10.1093/bioinformatics/btp616
31. McCarthy DJ, Chen Y, Smyth GK. Differential expression analysis of multifactor RNA-Seq experiments with respect to biological variation. *Nucleic Acids Res*. 2012;40(10):4288–4297. doi:10.1093/nar/gks042
32. Anders S, Huber W. Differential expression analysis for sequence count data. *Genome Biol*. 2010;11(10):R106. doi:10.1186/gb-2010-11-10-r106
33. Miguel RDV, Maryak SA, Cherpes TL. Brefeldin A, but not monensin, enables flow cytometric detection of interleukin-4 within peripheral T cells responding to ex vivo stimulation with Chlamydia trachomatis. *J Immunol Methods*. 2012;384(1–2):191–195. doi:10.1016/j.jim.2012.07.018
34. Gurnell M, Wentworth JM, Agostini M, et al. A dominant-negative peroxisome proliferator-activated receptor γ (PPARγ) mutant is a constitutive repressor and inhibits PPARγ-mediated adipogenesis. *J Biol Chem*. 2000;275(8):5754–5759. doi:10.1074/jbc.275.8.5754
35. Schuligoi R, Sturm E, Luschnig P, et al. CRTH2 and D-type prostanoid receptor antagonists as novel therapeutic agents for inflammatory diseases. *Pharmacology*. 2010;85(6):372–382. doi:10.1159/000313836
36. Galván-Peña S, Leon J, Chowdhary K, et al. Profound Treg perturbations correlate with COVID-19 severity. *Proc Natl Acad Sci*. 2021;118(37):e2111315118. doi:10.1073/pnas.2111315118
37. Roncati L, Nasillo V, Lusenti B, Riva G. Signals of Th2 immune response from COVID-19 patients requiring intensive care. *Ann Hematol*. 2020;99(6):1419–1420. doi:10.1007/s00277-020-04066-7
38. Nobs SP, Natali S, Pohlmeier L, et al. PPARγ in dendritic cells and T cells drives pathogenic type-2 effector responses in lung inflammation. *J Exp Med*. 2017;214(10):3015–3035. doi:10.1084/jem.20162069
39. Nagata K, Tanaka K, Ogawa K, et al. Selective expression of a novel surface molecule by human Th2 cells in vivo. *J Immunol*. 1999;162(3):1278–1286. doi:10.4049/jimmunol.162.3.1278
40. Grover P, Goel PN, Greene MI. Regulatory T cells: regulation of identity and function. *Front Immunol*. 2021;12:750542. doi:10.3389/fimmu.2021.750542
41. Skrzydlewska E, Łuczaj W, Biernacki M, et al. Preliminary comparison of molecular antioxidant and inflammatory mechanisms determined in the peripheral blood granulocytes of COVID-19 patients. *Int J Mol Sci*. 2023;24(17):13574. doi:10.3390/ijms241713574
42. Hotchkiss RS, Monneret G, Payen D. Sepsis-induced immunosuppression: from cellular dysfunctions to immunotherapy. *Nat Rev Immunol*. 2013;13(12):862–874. doi:10.1038/nri3552
43. van der Poll T, van de Veerdonk FL, Scicluna BP, Netea MG. The immunopathology of sepsis and potential therapeutic targets. *Nat Rev Immunol*. 2017;17(7):407–420. doi:10.1038/nri.2017.36
44. Reddy K, Sinha P, O'Kane CM, Gordon AC, Calfee CS, McAuley DF. Subphenotypes in critical care: translation into clinical practice. *Lancet Respir Med*. 2020;8(6):631–643. doi:10.1016/s2213-2600(20)30124-7
45. Bidar F, Hamada S, Gossez M, et al. Recombinant human interleukin-7 reverses T cell exhaustion ex vivo in critically ill COVID-19 patients. *Ann Intensiv Care*. 2022;12(1):21. doi:10.1186/s13613-022-00982-1
46. Zhou R, KKW T, Wong YC, et al. Acute SARS-CoV-2 infection impairs dendritic cell and T cell responses. *Immunity*. 2020;53(4):864–877.e5. doi:10.1016/j.immuni.2020.07.026
47. Snyder A, Jedreski K, Fitch J, et al. Transcriptomic profiles in children with septic shock with or without immunoparalysis. *Front Immunol*. 2021;12:733834. doi:10.3389/fimmu.2021.733834
48. Xu J, Li J, Xiao K, et al. Dynamic changes in human HLA-DRA gene expression and Th cell subsets in sepsis: indications of immunosuppression and associated outcomes. *Scand J Immunol*. 2020;91(1):e12813. doi:10.1111/sji.12813
49. Gil-Etayo FJ, Suàrez-Fernández P, Cabrera-Marante O, et al. T-helper cell subset response is a determining factor in COVID-19 Progression. *Front Cell Infect Microbiol*. 2021;11:624483. doi:10.3389/fcimb.2021.624483
50. Gil-Etayo FJ, Garcinuño S, Utrero-Rico A, et al. An early Th1 response is a key factor for a favorable COVID-19 evolution. *Biomedicines*. 2022;10(2):296. doi:10.3390/biomedicines10020296
51. Jung E, Cohen AJ, Howell R, et al. A dual role for CRTH2 in acute lung injury. *bioRxiv*. Published online 2022:2022.05.29.493897. doi:10.1101/2022.05.29.493897
52. King MR, Ismail AS, Davis LS, Karp DR. Oxidative stress promotes polarization of human T cell differentiation toward a T helper 2 phenotype. *J Immunol*. 2006;176(5):2765–2772. doi:10.4049/jimmunol.176.5.2765
53. Moghaddam AE, Gartlan KH, Kong L, Sattentau QJ. Reactive carbonyls are a major Th2-inducing damage-associated molecular pattern generated by oxidative stress. *J Immunol*. 2011;187(4):1626–1633. doi:10.4049/jimmunol.1003906
54. Ruskowski K, Neb H, Talbot SR, et al. Persistently elevated plasma concentrations of RIPK3, MLKL, HMGB1, and RIPK1 in patients with COVID-19 in the intensive care unit. *Am J Respir Cell Mol Biol*. 2022;67(3):405–408. doi:10.1165/rcmb.2022-0039le
55. Basu A, Ramamoorthi G, Albert G, et al. Differentiation and regulation of TH cells: a balancing act for cancer immunotherapy. *Front Immunol*. 2021;12:669474. doi:10.3389/fimmu.2021.669474
56. Stark JM, Tibbitt CA, Coquet JM. The metabolic requirements of Th2 cell differentiation. *Front Immunol*. 2019;10:2318. doi:10.3389/fimmu.2019.02318
57. Nobs SP, Kopf M. PPAR-γ in innate and adaptive lung immunity. *J Leukoc Biol*. 2018;104(4):737–741. doi:10.1002/jlb.3mr0118-034r
58. Wu J, Wang Y, Zhou Y, et al. PPARγ as an E3 Ubiquitin-Ligase impedes phosphate-Stat6 stability and promotes prostaglandins E2-mediated inhibition of IgE production in asthma. *Front Immunol*. 2020;11:1224. doi:10.3389/fimmu.2020.01224

59. Chu CM, Cheng VCC, Hung IFN, et al. Role of lopinavir/ritonavir in the treatment of SARS: initial virological and clinical findings. *Thorax*. 2004;59(3):252. doi:10.1136/thorax.2003.012658
60. Sheahan TP, Sims AC, Leist SR, et al. Comparative therapeutic efficacy of remdesivir and combination lopinavir, ritonavir, and interferon beta against MERS-CoV. *Nat Commun*. 2020;11(1):222. doi:10.1038/s41467-019-13940-6
61. Ogletree ML, Chiang KC, Kulshrestha R, Agarwal A, Agarwal A, Gupta A. Treatment of COVID-19 pneumonia and acute respiratory distress with Ramatroban, a thromboxane A2 and prostaglandin D2 receptor antagonist: a four-patient case series report. *Front Pharmacol*. 2022;13:904020. doi:10.3389/fphar.2022.904020
62. Sposito B, Broggi A, Pandolfi L, et al. The interferon landscape along the respiratory tract impacts the severity of COVID-19. *Cell*. 2021;184(19):4953–4968.e16. doi:10.1016/j.cell.2021.08.016
63. Theken KN, FitzGerald GA. Bioactive lipids in antiviral immunity. *Science*. 2021;371(6526):237–238. doi:10.1126/science.abf3192
64. Cloutier A, Marois I, Cloutier D, Verreault C, Cantin AM, Richter MV. The Prostanoid 15-Deoxy-Δ12,14-Prostaglandin-J2 Reduces Lung Inflammation and Protects Mice Against Lethal Influenza Infection. *J Infect Dis*. 2012;205(4):621–630. doi:10.1093/infdis/jir804
65. Gupta A, Chiang KC. Prostaglandin D2 as a mediator of lymphopenia and a therapeutic target in COVID-19 disease. *Méd Hypotheses*. 2020;143:110122. doi:10.1016/j.mehy.2020.110122
66. Shahzad S, Willcox M. Immuno-pathogenesis of nCOVID-19 and a possible host-directed therapy including anti-inflammatory and anti-viral prostaglandin (PG J2) for effective treatment and reduction in the death toll. *Méd Hypotheses*. 2020;143:110080. doi:10.1016/j.mehy.2020.110080
67. Meng H, Sengupta A, Ricciotti E, et al. Deep phenotyping of the lipidomic response in COVID-19 and non-COVID-19 sepsis. *Clin Transl Med*. 2023;13(11):e1440. doi:10.1002/ctm2.1440
68. Wong LYR, Zheng J, Wilhelmsen K, et al. Eicosanoid signalling blockade protects middle-aged mice from severe COVID-19. *Nature*. 2022;605(7908):146–151. doi:10.1038/s41586-022-04630-3